SYNTHESIS AND CHARACTERIZATION OF IRON OXIDE FROM CLAY ORE FOR BIOMEDICAL APPLICATIONS

ASHESI UNIVERSITY

CAPSTONE PROJECT

B.Sc. Mechanical Engineering

REBECCA AGIDI

(ID #: 76642021)

SUPERVISOR: DR. YIPORO DANYUO

MAY 2021

ASHESI UNIVERSITY

SYNTHESIS AND CHARACTERIZATION OF IRON OXIDE FROM CLAY ORE FOR BIOMEDICAL APPLICATIONS

CAPSTONE PROJECT

Capstone Project submitted to the Department of Engineering, Ashesi University in partial fulfilment of the requirements for the award of Bachelor of Science degree in Mechanical Engineering.

REBECCA AGIDI

DECLARATION

I hereby declare that this capstone is the result of my own original work and that no part of it has been presented for another degree in this university or elsewhere.

Candidate's Signature:

……

Candidate's Name:

……

Date:

……

I hereby declare that preparation and presentation of this capstone were supervised in accordance with the guidelines on supervision of capstone laid down by Ashesi University.

Supervisor's Signature:

……

Supervisor's Name:

……

Date:

……

Dedication

This report is dedicated to my adorable parents; Agidi and Monica, and to my siblings; Goodness, Salome, Emmanuel and Marvelous.

Acknowledgements

To begin with, I would like to thank God for sailing me through this project successfully.

I would also like to express my sincere gratitude to my supervisor, Dr. Danyuo Yiporo, for his timely support, patience, and guidance.

My appreciation is also extended to Joseph Timpabi and Peter Kwao for their technical support at the mechanical lab and workshop.

To my friends, Emmanuel David, and Ebenezer John, thank you for your regular encouragement. Additionally, I would like to extend my profound gratitude to my family for their prayers and support throughout my studies.

Finally, a big thumbs up to you Rebecca, for making this happen!

ABSTRACT

The purpose of this project is to synthesise and characterize iron from clay ore which would be used in biomedical applications. Two sources of clay samples were obtained from the Savannah and Volta Region for the studies. The clay sample from the Savannah Region revealed a milky colour, while the clay sample from the Volta Region had red colour. The as-received clay was characterized with X-ray fluorescent (XRF) spectroscopy to determine the major oxides and elemental compositions. The results from the XRF studies shows that, the Savannah and the Volta clays contains 10.2 mass%, and 8.49 mass% hematite (Fe_2O_3). Iron synthesis was achieved via chemical leaching with phosphoric acid, and hydrochloric acid. The leached substance was analysed with ultraviolet visible (UV-Vis) spectroscopy. Kinetics of iron released was analysed using kinetic modules such as Zeroth order, First order, Second order, and Higuchi model. The results agreed with the Zeroth and Second model with a linear fit and regression coefficient, $R^2 = 0.994$ and $R^2 = 0.998$ respectively. The iron in solution was precipitated from solution using sodium hydroxide to enhance the yield of the iron. The implications of the results were discussed for the synthesis and further characterization of conjugated iron nanoparticles for biomedical applications.

Table of Content

List of Figures

List of Tables

CHAPTER ONE

1.0 Introduction

1.1.Introduction and Background Studies

Clays contribute to the formation of soil structure by undergoing seasonal shrinking and swelling [1]. They are fine-grained particles and possess minerals in them. Clay minerals are called secondary silicates formed from weathering of primary rock-forming minerals [2]. The minerals within clay belong to the phyllosilicate family of minerals, characterized by their layered structures. The mineral layers composed of polymeric sheets of silica tetrahedra attached with octahedral sheets [2], [3]. Essentially, clay minerals composed of silica, alumina, or magnesia or both, and water, but iron substitutes for aluminum and magnesium in varying degrees, and appreciable quantities of potassium, sodium, and calcium are frequently present as well [3].

Clay minerals are classified based on the variations of chemical composition and atomic structure into nine groups [3]. They include:

- Kaolin-serpentine-examples are kaolinite, halloysite, lizardite, amd chrysotile.
- Pyrophyllite-talc.
- Mica- examples are illite, glauconite, and celadonite.
- Vermiculite.
- Smecite – examples are montmorillonite, nontronite, and saponite.
- Chlorite – examples are sudoite, clinochlore and chamosite.
- Sepiolite – palygorskite.

- Interstratified clay minerals – examples are rectorite, corrensite, and tosudite.
- Allophane – imogolite.

Clay minerals are of immense value to our building industries, the materials and manufacturing industries, ceramic industry, the environment, etc. [4], [5]. The presence of iron in the structures of clay minerals infuses an additional facet into their importance [5].

Iron oxide minerals that are dominant give the clay its characteristic colour [6]. They can be removed from their impurities using either physical or chemical method. Chemically removing (leaching) the irons from the clay ore is said to be efficient [6]. Acids, such as phosphoric, hydrochloric, and sulfuric acid are solvents that can be used in the leaching process. Phosphoric acid, from literature, removes the most iron from the clay ore.

Iron is essential for cell replication, metabolism, and growth in the human body [7]. Research has proved the function of Iron oxide as a progressive remedy for cancer [7]. Cancer is a disease that occurs when cells divide and multiply uncontrollably thereby destroying the normal body tissues and surrounding cells [8] , [9]. The leading cause of death is the World today is cardiovascular diseases [10] followed by breast cancer [11]. Early detection of cardiovascular cancer, lung cancer, breast cancer, etc. before the disease cells metastasis is key to positive treatment outcomes.

Chemotherapy, surgery, and radiotherapy are the current conventional treatment methods of cancer but have proved to have side effects. They are non-targeting and lacks specificity [12]. Chemotherapy for example uses highly toxic drugs due to the aggressive nature of cancer which leads to side effects such as vomiting, fatigue, destruction of hair cells, lack of taste, and destruction of other important body cells [13]. Surgery on the other hand does not guarantee the removal of residual cancer cells after surgery. Hence, post-surgery may lead to the spread of cancer to other parts of the body. This, therefore, required injectable

nanoparticles, or functionalized nanoparticles which could be used to induce laser heating for successful cancer eradication. It might also be known that radiation can promote cancer development through mutation of cells [14]. Hence, it is not recommended for a person to undergo radiation therapy for more than two times in a year [14]. For example, there is a high probability that young girls who undergo chest X-Ray may develop breast cancer in their lifetime [14], [15].

Nanoparticles (NPs) of iron oxide (magnetite) has proved to be a better therapy in the localized delivery of drugs [16]. Iron-based NPs have been extensively investigated due to their excellent superparamagnetic, biocompatible, and biodegradable properties [17], [18].

This paper will focus on removing iron (magnetite) from clay ore by leaching. Phosphoric acid, hydrochloric acid and sulfuric acid will be used in the leaching process from two sourced clays (from the savannah Region and Volta region of Ghana). The iron would be precipitated from solution using sodium hydroxide to obtain a better yield of the iron. The leached substance, the residue, will then be characterized.

1.2 Problem Definition

According to the World Health Organization, cancer is currently the second leading cause of death, worldwide, after cardiovascular diseases [11]. Current trends also suggest that cancer would become the leading cause of death by 2030 [11], [19]. Bulk chemotherapy and radiotherapy, are the current methods used in delivering cancer drugs, have varied side effects. Radiation therapy can result in side effects such as diarrhoea, swelling, nausea, vomiting and many more, depending on the part of the body being treated [20]. Therefore, human life is in danger of further disorders leading to complications as far as death. It

imperative that a better and cost-effective method of administering treatment to the disease is obtained, which will minimize the risk of death associated to cancer.

More than 80% of African health care systems have inadequate facilities to provide accurate therapeutics and diagnosis on cancer due to the low level of knowledge in biomaterials for health solutions [9]. Most communities in Africa resort to local herbs for cancer treatment. These herbs may impede cancer growth for some time, but cancerous cells could regenerate.

Africa is endowed with a lot of minerals. However, exploitation has been ineffective. Clay mineral are in abundant in Ghana, but mineral extraction such as iron form clay has been understudied. The field of nanotechnology in medicine has great opportunities in our next generation of cancer detection and treatment. Extraction of minerals from clay stands as an ever-growing field of endeavour in a wide range of biomedical application [9], [21]. X-ray diffraction (XRD) and X-ray fluorescent (XFR) spectroscopy showed clays in Ghana contained a wide variety of major oxides and minor minerals.

1.3 Motivation

Africa is considered to have a large proportion of the world's natural resources, yet it fails to transform them into a final product that will serve as a source of income. This contributes to the challenge in the economic growth and development of Africa [22]. Also, most of the youth are unemployed because of the lack of technological knowledge.

Adding value to our clay ores, abundant natural resource, will resort to varied opportunities in the nation as well as a means of revenue for the nation since a product (magnetite) from it is essential for the cure of a deadly disease such as cancer. Primary materials such as clay ore is in abundance and the only cost involved in acquiring it is the digging fee and

transportation fee to the laboratory. Also, the process of leaching used available acids (such as sulfuric acid, phosphoric acid and hydrochloric acid) which are of moderate cost.

1.4 Justification

Nanotechnology is the engineering and manufacturing of materials at the atomic and molecular scale. Its structure is within the 1-100 nm size [23]. Nanotechnology is one of the emerging technologies that is having a great impact in all industrial sectors [24]. With the use of nanotechnology, materials can be made lighter, more reactive, stronger, and more durable. Nanoscale materials now allow washable, durable "smart fabrics" equipped with flexible nanoscale sensors and electronics with capabilities for health monitoring [25].

"Nanotechnology's ability to shape matter on the scale of molecules is opening the door to a new generation of diagnostics, imaging agents, and drugs for detecting and treating cancer at its earliest stages" [26]. The use of the current treatment of cancer, that is the chemotherapy and radiotherapy, are less effective when administering to patients. These anticancer drugs are non-specific. They tend to not differentiate between normal and malignant cells, thereby leading to side effects [12]. Research is being conducted to come up with a therapy where a nanoparticle can deliver medication directly to cancer cells to minimize the risk of damage to healthy tissues. Thus, reducing drastically the side effects of chemotherapy [25], [26], [12].

1.5 Goal and Specific Objectives

The goal of this capstone project is the characterization and extraction of iron oxide from clay ores. The goal would be accomplished with the following milestone objectives:

- Using mechanical methods to achieve communition processes (reducing the larger lumps of the clay samples to finer particles) and particle size analysis.
- Elemental analysis for the presence of major oxides using XRD and XRF.
- Synthesis of iron from clay ores by the chemical leaching method.
- Characterization and quantification of iron concentration using ultraviolet visible (UV-vis) spectrometer at different acid concentrations and effect of leaching time.
- Optical analysis on the porosity of the clays and particles distribution.
- Study the kinetics of the leaching processes: studying the relationship between concentration and time using zeroth order, first order, second order, and Higuchi model.
- Precipitation of iron using sodium hydroxide.
- Mechanical determination of compressive properties of the clay (flexural strength, flexural modulus, peak loads, etc)

1.6 Expected Outcomes

This project will enhance the use of clay as a source of iron for biomedical application. In accomplishing the project, two different samples of clay are crushed into fine particles to enhance the liberation of the iron in solution using a chemical method known as leaching. The effect of chemical type and acid concentration would be investigated. The kinetics of leaching would be extensively studied. Elemental analysis is done using XRD and XRF to determine the major and minor oxides present in the samples. Implications of the results will be discussed for the evaluation of the iron. Moreover, this method will provide a cost-effective means of extracting iron for further applications.

CHAPTER TWO

2.0Literature Review

2.1 Introduction

Clay has varied mineral compositions with each having a given percentage that makes them possess different properties. Their unique crystal structures give clay materials special properties [2]. These properties include cation exchange capabilities, plastic behaviour when wet, catalytic abilities, swelling behaviour, and low permeability [1], [3]. To acknowledge all the features of clay and clay-based minerals, the understanding of their properties especially the cation exchange capability is important in the sense that it affects the mechanical and physical properties of the clay. The iron oxide in the clay gives off different colour shades depending on the amount of oxide present. Research has proved that iron oxide nanoparticles (NPs) with nanocrystalline magnetite (Fe_3O_4) cores have great potential for use in oncological medicine due to their biocompatibility, biodegradability, facile synthesis, and ease with which they may be tuned and functionalized for specific applications [16], [17]. Magnetite-core NPs have seen widespread development by research teams throughout the world, yet few formulations have been approved for clinical uses [16].

The conventional treatment of cancer such as chemotherapy and radiotherapy have side effects. These conventional methods of cancer treatment lack specificity and are non-targeting and hence affects non-target tissues/cells [12], [13]. The goal of chemotherapy is to impede the growth of tumor cells through the action of chemicals that inhibit cell function. Drugs have been developed to attack cell function in several ways, including the disruption of DNA replication and repair, interfering with protein expression, and other mechanisms of stopping or inhibiting cell division [13]. However, the efficacy of chemical drugs acting

alone is limited due to their lack of selectivity in targeting cancer cells, pharmacological limitations, and their toxicity to healthy tissues [12], [16]. Encapsulating or attaching molecular drugs to NPs helps to selectively deliver chemotherapeutics to target sites, allowing for increased dosage, minimizes off-target toxicity, protects drugs from degradation, and enhances biocompatibility [12], [25], [26].

Nanoparticles also known as ultrafine particle, is said to be between 1 and 100 nm in diameter. The particles have wide variety of potential applications in optical, biomedical, and electronic fields. Nanoparticles are being increasingly used in drug delivery systems. Cancer drugs should be able to reach the desired tumour tissues through penetration of berries in the body with minimal loss of their volume or activity in the blood circulation as well as selectively killing tumour cells without affecting normal cells. Nanoparticles of iron oxide has proved to be a better therapy in the localized delivery of drugs [16].

2.2 Clay mineral deposits

Clay and clay minerals occur under limited range of geological conditions [27]. A number of these clays form where rocks meet with water, air, or steam. Some of these situations include sediments on sea or lake bottoms, rocks in contact with water heated by magma (molten rock), and deeply buried sediments containing pore water, causing the formation of clay minerals from pre-existing minerals [1] [2]. They have proven to be part the most essential industrial minerals because of their unique physicochemical properties and varied applications within a wide range of fields including ceramics, construction, environmental remediation, and biomedical as well as cosmetics [28]. Clays can exchange ions by attracting them to their surfaces and taken up within the structure of these minerals [3].

In Ghana, despite the abundance of clay deposits which have important domestic applications, their physiochemical properties have not been fully explored. The use of clay goes from traditional uses like geophagy to contemporary use in pottery, construction, and water purification. Each region in Ghana has a measure of clay deposits which have unique properties that can be fitted towards a particular application [28]. Below gives properties of some clay deposits from some regions in Ghana [28]. Some properties of clay deposits from regions in Ghana are presented in appendix A.

Fe_2O_3, TiO_2, K_2O, and Na_2O are some impurities that vary among clay samples in various localities in Ghana. The presence of certain elements like Fe in the clay mineral gives the clay its colour. For instance, "Fe^{2+} can convert to Fe^{3+} through oxidation which are the common isotopes of iron present in soils and can confer their coloration to clay" [28]. Also, chemical interaction of organic compounds with clay minerals influences the colour of the clay.

2.3 Types of Iron minerals

Iron is the most common metallic element on earth. It is dark, silvery grey in colour when it is in the pure. Iron is very reactive and easily oxidizes. Iron occurs mainly in iron-oxide ores. Some ores have minerals rich in iron whereas others are less rich in iron which have several impurities. The impurities lower the value of the iron ores. For instance, sulphur in the ore makes the iron and steel brittle. Some of the major irons found in ores are presented in **Table 2.2.**

Table 2.1: Different types of major irons [29].

Name	Chemical Formula	Weight% (Fe)
Magnetite	Fe_3O_4	72.36
Hematite	Fe_2O_3	69.94
Goethite	FeO(OH)	62.58
Limonite	FeO(OH). n(H_2O)	52 (n =1)
Siderite	$FeCO_3$	48.2
Bog iron	Limonite plus dirt	_
Pyrite	FeS_2	46.5

2.3.1 Magnetite

Magnetite is a mixture of Iron (II) oxide and iron (III) oxide (Fig.). The mineral magnetite has higher iron content than hematite. However, while hematite ore generally contains large concentrations of hematite, magnetite ore generally holds low concentrations of magnetite. As a result, this type of iron ore must be concentrated before it can be used to produce steel. The magnetic properties of magnetite ores are helpful during this process. The end products from magnetite ore are of higher quality compared to that of the hematite ore though it requires more treatment. Due to the less impurities in magnetite ore than in hematite ore, the elevated cost of processing magnetite ore can be balanced out.

2.3.2 Hematite

Deposits of considerable quantity have been found at the contacts of igneous intrusions, generally basic, with crystalline limestone, dolomite, and limey shale; the ore is usually of the specular variety, and it is partly magnetite. Hematite ore is a naturally high iron content. Because of its high iron content, hematite ore must undergo only a simple crushing, screening, and blending process before being shipped off for steel production. The most important hematite deposits are of a sedimentary origin, the ore forming beds in stratified rocks. Also, hematite is found as the dominant mineral, whereas quartz and kaolinite are as gangue minerals in low-grade iron ore [30].

2.3.3 Limonite

Limonite also known as brown ore, Fig 3, is found at the bottom of some bogs and shallow lakes, in favorable situations, where the weathering rocks have yielded iron to the water draining into these basins. Considerable deposits of limonite have been found in places where there is no standing water at present. Limonite is sometimes formed in large quantities by the weathering of the sulphides of iron; such gossan has occasionally been used as an iron ore.

2.3.4 Siderite

It is usually grey or white, as seen in Fig 4; but at the surface it weathers to limonite, and the weathering may extend to a considerable depth. A rusty capping may cover a deposit of siderite. Where the ore forms the face of a cliff, the limonite may wash away as fast as it forms, leaving the siderite clean.

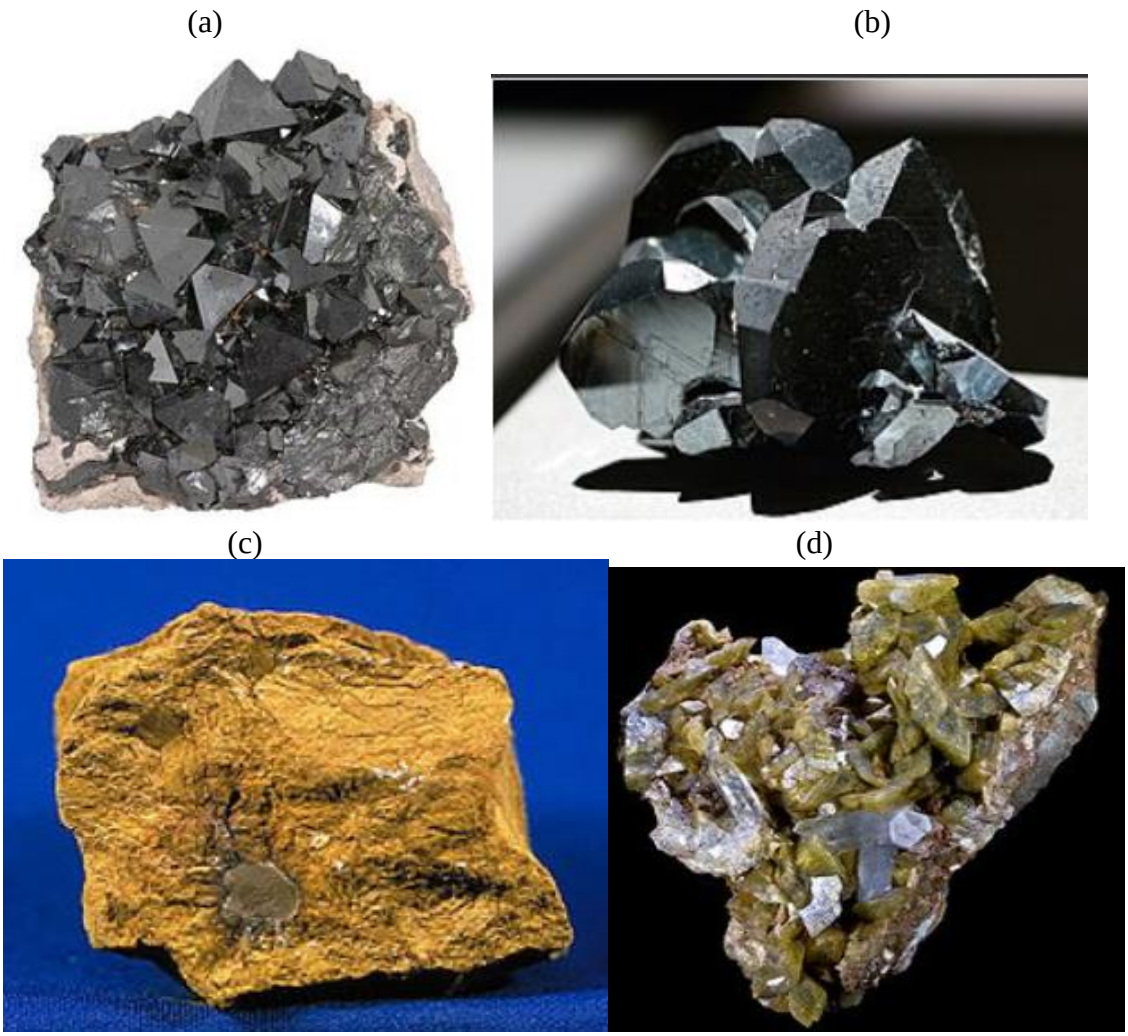

Figure 2.1: Sample Iron Ores: (a) Magnetite, (b) Hematite, (c) Limonite, and (d) Siderite.

2.4 Iron ore mining

Mining allows the extraction of the important commodity which is in high demand due to infrastructure growth and population in the developing countries. Surface (open pit) mining and underground (shaft) mining are the two basic methods of mining. Surface mining is the preferred choice, though there are some exceptions, because it is cheaper.

2.5 Iron ore processing

Iron ore occurs naturally in a variety of forms, from sand-like iron fines to solid rock masses. Crude ore, or ore mined in the natural state, occasionally occurs in a pure state, and requires some form of beneficiation. Crude ore is commonly mixed with other minerals (gangue), which reduce the iron content. Crude iron ore is classified in three general categories:

- **Direct Shipping**: These ores are transported as mined. They are generally composed of hematite, magnetite, goethite, etc.
- **Concentrates:** Iron ore known as low-grade, intermediate, taconite, or concentrating ore require further treatment to upgrade the iron content. Improving its quality is referred to as beneficiating.
- **Agglomerated**: The process of amassing material fines into cohesive units like pellets or granules. The pellet is the major form of introducing iron into the steelmaking blast furnace [31].

2.6 Crushing and Grinding

Mined iron ore contains lumps of varying size, the biggest being more than 1 metre (40 inches) across and the smallest about 1 mm (0.04 in). However, blast furnace, requires lumps between 7 and 25 mm, so the ore must be crushed to reduce the maximum particle size [32]. It aids in the liberation of the iron minerals from the main material (rock).

2.7 Hydrometallurgy

Hydrometallurgy is a technique within the field of extractive metallurgy which involves the use of aqueous solution for the recovery of metals from ores. The solutions being used in the metal resources depletion is an efficient extraction of low-grade ores, and the retrieving of valuable metals from urban mining [33]. Hydrometallurgy consists of three processes: leaching; solid or liquid separation and purification; and metal recovery.

Leaching is the dissolution of the solid material in a given solvent through a selected procedure. The metal-bearing components dissolve, while the other components do not. There is separation of the solution from the unaffected solids which results in the separation of the metal from the unwanted components in the feed material [34].

The solution gotten from leaching still has impurities in that needs to be removed. Sometimes, the concentration of the desired metal is too low, and some form of concentration needs to be applied before the metal can be extracted. Thus, the concentration or purifying process of a metal-bearing solution can be accomplished using evaporation method, precipitation process and a process that utilizes a carrier phase. The metal is visible to be removed after purification.

Hydrometallurgical treatment makes it possible to limit the environmental impacts like residual waste producing, energetic expenditure and reagent consumption.

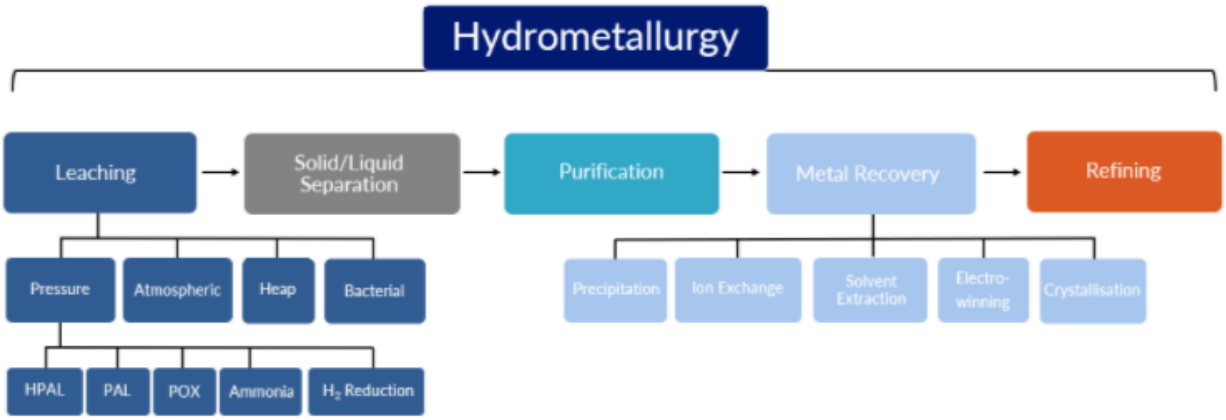

Figure 2.2: Hydrometallurgy process [35]

2.8 Mechanical Characterisation of the Clay Ore

2.8.1 Flexural strength

Flexural strength (σ_F) is a measure of the tensile strength of an unreinforced concrete beam to resist failure in bending as illustrated (Fig.). It is useful in knowing the quality of concrete work done.

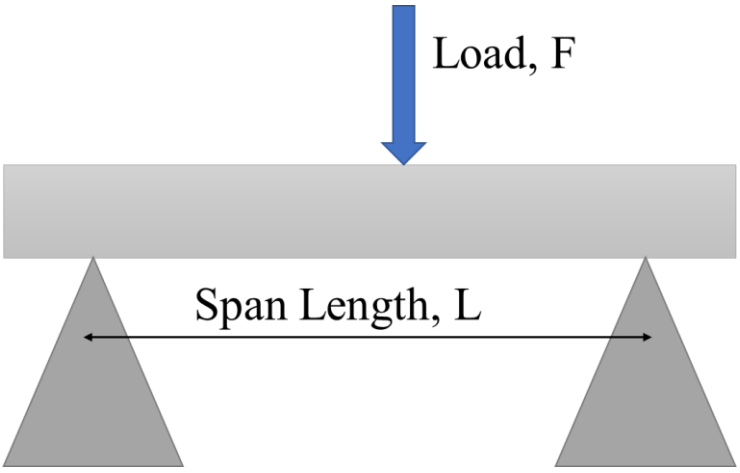

Figure 2.3: Illustration of Flexural or Bending Testing.

Flexural Strength is determined by:

The formula used to calculate the flexural strength under axial force (from a rectangular sample) is given by [36] :

$$\mathfrak{e} = \frac{3FL}{2bd^2}$$

where F is the load (force) (N) at the fracture point, L is the length of the support span length, b is the width of the sample, and d is the thickness.

2.8.2 Flexural Modulus

Flexural Modulus (E_f) is the tendency of a material to resist bending. The flexural modulus and deflection are respectively given by the formulas [36]:

$$E_f = \frac{L^3 F}{4ba^3 \delta} \ (N/m^{-2}) \qquad (2.2)$$

$$\delta = \frac{L^3 F}{48IE} \qquad (2.3)$$

where the second moment of inertia, I = $\frac{1}{12} ba^3$, F is the load (force) at the fracture point (N), L is the distance between the two outer supports (span length), b is width, a is the height, and δ is the deflection.

2.9 Characterization Techniques for the Detection of Iron

It is only right to know what a material is composed of. The structural, physical, and chemical characteristics of clay minerals are related to their applications. Thus, the physical and chemical properties of clay minerals dictate their utilization in the process industries as

well as beneficiation needed before it is used [37] . Knowledge on this, has further heightened industrial development.

Also, characterization of most clay minerals provides sufficient data to compare, analyse and draw conclusions for further studies. There are various characterization techniques that are used which will be expanded on.

2.9.1 X-Ray Diffraction (XRD)

XRD is a technique used to characterize the nature of materials, especially its crystallinity, chemical composition, and physical properties of materials. The phases are identified by comparison of the acquired data to that in the reference databases. The XRD analysis is done with an X-ray source of Cu Kα radiation [38]. XRD is useful in evaluating minerals, polymers, corrosion products and unknown materials.

2.9.2 X-Ray Fluorescence (XRF)

XRF is an analytical technique used to determine the elemental composition of a material. "XRF is based on the principle that individual atoms, when excited by an external energy source, emit X-ray photons of a characteristic energy or wavelength" [39] . A set of characteristic fluorescent X-rays is produced by each of the elements in the sample which is unique for that element. XRF is often used to authenticate XRD data and otherwise [40]

XRF has two main types of detectors; the wavelength dispersive detection and the energy dispersive detection are used for decomposition of the fluorescent radiation in the spectra.

2.9.3 Fourier Transform Infrared Spectroscopy (FTIR)

FTIR is an effective analytical instrument for detecting functional groups and characterizing covalent bonding information. It identifies chemical bonds in a molecule by producing an infrared (IR) absorption spectrum. [41] "The IR spectrum of a clay mineral is sensitive to its chemical composition, isomorphous substitution, layer stacking order, or structural modifications. This makes FTIR spectroscopy the most informative single technique not only for clay mineral composition and structure but also for interactions of the clay minerals with inorganic or organic compounds [42].

2.9.4 UV-Vis Spectroscopy

Ultraviolet visible (UV-Vis**) s**pectroscopy is the measure of the absorbance or transmittance of light passing through a medium as a function of wavelength. UV-Vis is an inexpensive, simple, non-destructive, analytical method appropriate for a wide class of organic compounds and some inorganic species. It is used to derive liquid phase reaction kinetics, and to identify the mechanism at the molecular scale by chemical engineers for qualitative analysis. Moreover, it helps to identify and quantify the concentration of compounds in liquid streams. The UV-vis diffuse reflectance spectroscopy has enhanced scattering properties that measures the properties of solids and powders [43].

Beer-Lambert Law is the principle behind absorbance spectroscopy which is given by:

$$A = \log\left(\frac{I_o}{I}\right) = \varepsilon C l$$

where A is absorbance, I_o is the intensity of light incident upon sample cell, I is the intensity of light leaving the sample cell, C is the concentration of solution, l is the path length of the sample cell, and ε is the molar absorptivity.

CHAPTER THREE

3.0 Materials and Methods

3.1. Materials

The clay ore materials used for the synthesis of iron oxide was dug out from the ground in different regions in Ghana. The red coloured clay (Fig.3.1a) was sourced from the Volta Region of Ghana, whereas the grey coloured clay (Fig.3.1b) was obtained from the Savanna Region. Two different acids were procured and used to leach the iron from the clay ore. Diluted phosphoric acid (H_3PO_4) and Diluted hydrochloric acid were procured from Finap Enterprise (*Kokomelmle,* Accra, Ghana).

Mortar and pestle, and a sieve were used also provided by the engineering workshop, Ashesi University. The experiments were carried out at the Research Building (RB), Biology and Chemistry Laboratory at Ashesi University, Ghana. Sodium hydroxide, filter paper and syringes were supplied by the Biology and Chemistry Lab of the Research Building Laboratory at Ashesi University.

(a) (b)

Figure 3.1: As-Received Clay Samples: (a) Lumps of Volta Clay and (b) Lumps of Savannah Clay.

3.2 Experimental Procedures

3.2.1 Comminution Process

Comminution process (Fig.3.2) was first carried out in the as-received clay ores. The lumps of clay samples were crushed to smaller particle size using a mortar and a pestle (Fig. 3.2b-d). A sieve was used to further arrive at a finer particle size. The aim was to increase the concentration of the iron in the ore. Smaller particles have surface areas that enhances the leaching process. The comminution process was carried out in the mechanical workshop at Ashesi University.

(a) (b) (c) (d)

Figure 3.2: Comminution Process: (a) Lumps of Clay, (b) Crushing Using an Improvised Mortar and Pestle to Reduce Solid Particle Size, (c) the Sieve Type Used, and (d) Fine Particles of Clay.

3.2.2 **Optical Characterization and Particle Size Determination**

Optical analysis was carried out on the as-received clay using a scanning electron microscope (SEM) and a USB microscope (Fig. 3.3a). This helps to determine the packing density of the clay ores as well as supports its structural features such as porosity.

Particle size analysis on the screen samples was done using information from the sieve thickness and mesh counts. The thickness of the wire from the sieve (Fig. 3.3b) was used to determine the particles size (PS) of the sieved powders as given by:

$$\text{PS} = \frac{K}{MC} - t_w \tag{3.1}$$

where MC is the mesh count, which was determined to be 18, the thickness, t_w of the sieved wire was 0.5 mm, and the constant K was assumed to be 25.4 as adopted from lecture materials on the course, manufacturing processes under the topic of powder metallurgy. The average particles sizes were determined to be 911μm.

(a)

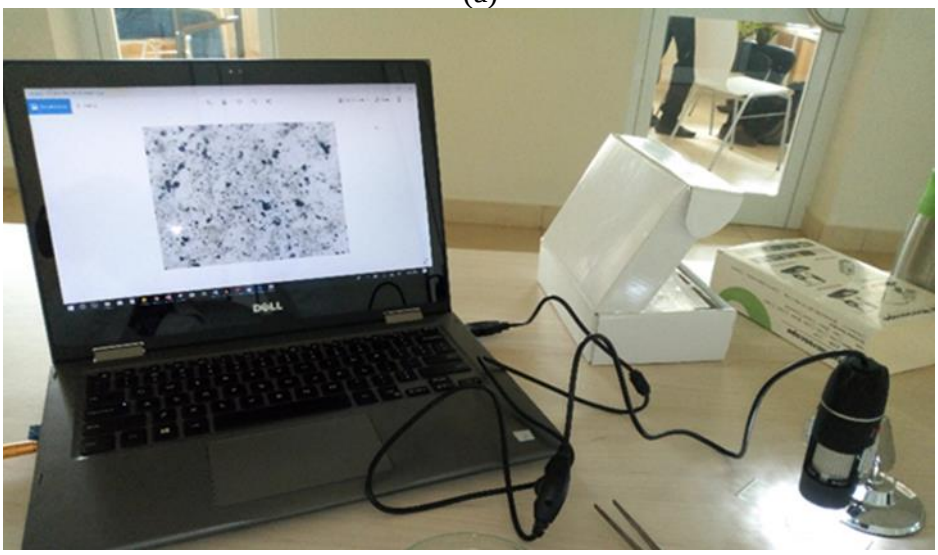

(b)

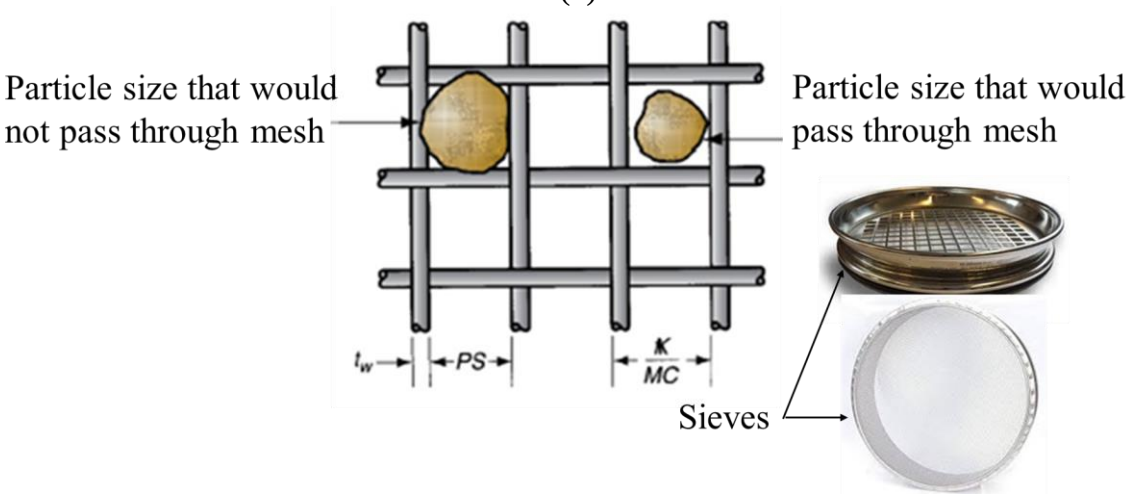

Figure 3.3: Optical and Particles Size Determination: (a) Imaging with a USB Microscope and (b) Screening Process for Particle Size Determination.

3.2.3 Chemical Leaching of Iron

To conduct leaching, a beaker and a hot plate with magnetic stirrer were used (Fig.3.4a). A 25 g of clay samples were determined using an electronic weighing balance (Kerro P3B/6002, 600 g / 0.01 g, India). The measured sample was added to the beaker at a

constant stirring of 500 revolutions per minute (rpm). Clay samples were diluted with 500 mL of the leaching acid. The hot plate provided the heat source, at a constant temperature of 94^{o}C. It had a thermo-regulator which helped to maintain the temperature. All leaching All leaching experiment lasted for two hours [44]. Concentrations of 1.0 M, 2.0 M, and 3.0 M were used, while keeping the temperature constant at 94^{o}C [45]. This was done to determine how the concentration of acid affects the removal of the iron from the clay ore.

A sample of 13 ml was pipetted from the leach slurry at 30 min interval and stored in a 15 ml tube as seen (Fig. 3.4b). The samples were then filtered using a Wetman filter paper and centrifuged at 3000 rpm for 5 min. 7 ml aliquot of the solution from the centrifuged samples (Fig. 3.4c) were collected for total iron determination as guided [44] using an ultraviolet-visible spectroscopy (UV-vis spectroscopy). Figure 3.4c shows a clear uniform solution that has been filtered and centrifuged for UV-vis analysis. The residue from the leached sample is filtered and dried under the Sun.

(a) (b) (c)

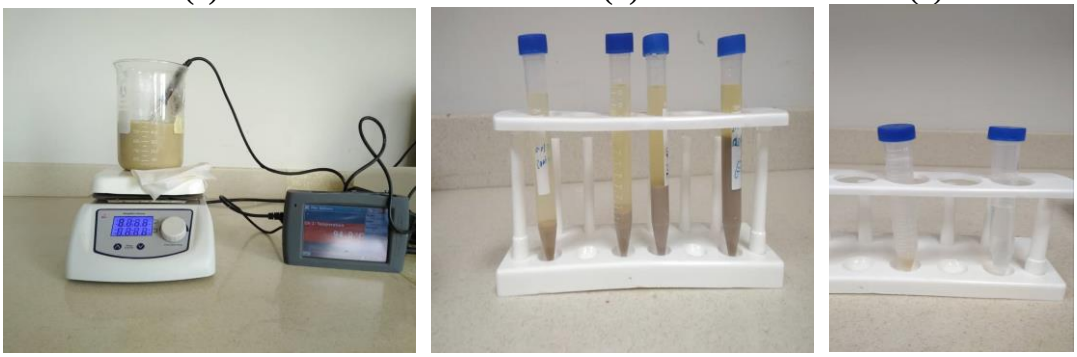

Figure 3.4: Synthesis of Iron from Clay Ores: (a) Leaching at a Constant Temperature, (b) 13 mL of the leach slurry Collected at 30 min Interval, (c) A Clear Content Obtained after Filtration and Centrifuging.

(a) (b)

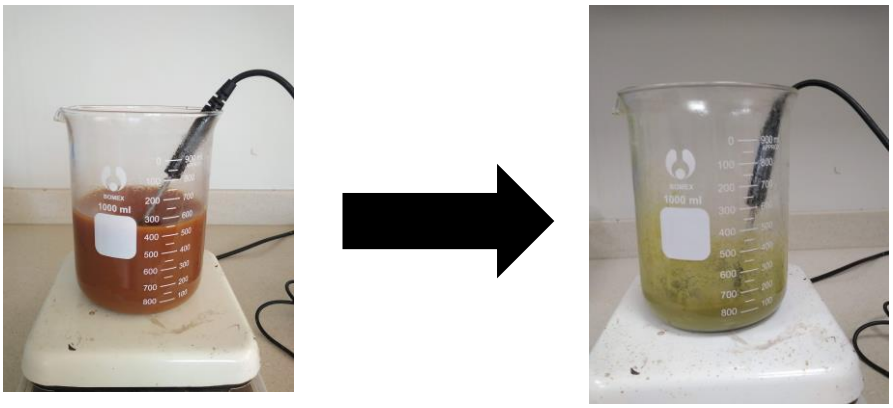

Figure 3.5: Leaching of Iron from the Volta Clay (a) Initial stage of leaching (b) Final stage of leaching

Figure 3.5 shows the leaching process conducted on the volta clay using phosphoric acid. Fig 3.5 (a) being the initial process of leaching at a constant temperature of 94^{o}C whereas, Fig. 3.5 (b) is the outcome of the leaching after 120 mins, which shows a change in colour of the clay and this agrees with literature [6], [28].

3.2.4 Sample Characterizations

Different characterization techniques were used to analyze the clay samples. X-Ray Diffraction (XRD) and X-Ray Fluorescence XRF) was used to measure the chemical and physical properties of the clay, and the elemental composition of the clay respectively. Fourier transform infrared (FTIR) spectrophones was used to determine the functional groups present in the clay. The absorbance of iron in a solution was achieved using UV-visible spectroscopy.

3.2.4.1 Fourier Transform Infrared Analysis

The functional groups were analyzed and determined with the FTIR. Spectra transmission versus wavenumber were plotted from 500 cm^{-1} to 4000 cm^{-1}. The analysis was done in the Chemistry Department Laboratory at the University of Ghana, Legon. Mapping with standards revealed the chemical bonds formed within the clay. Results were compared to the residue from the leached samples.

3.2.4.2 UV-Vis Spectroscopy

A UV-vis spectrophotometer was used to determine the absorbance. For samples leached with phosphoric acid, the blank was made of phosphoric acid. Similarly, HCL was used as the blank when UV-Vis was measured. The aliquot contains iron oxide. Clean cotton wool was used to wipe the transparent side of the cuvette to avoid dirt. The cuvette was carefully handled to avoid touching the smooth surface where the laser beam travels through. The UV-Vis machine (Jenway 7205, United Kingdom, Europe) was then initialized, and measurements were taken from 250 nm to 400 nm. The UV-Vis helps to determine the optical property of iron oxide in the solution.

The bandgap energy of synthesized particles was given by [46]:

$$E = \frac{hc}{\lambda} \tag{3.1}$$

where h is the plank's constant, c is the velocity of light, and λ is the wavelength.

Beer-Lambert's law allows for the characterization of the absorbance and concentration of iron leached. The formula that backs the law is given by:

$$C = \frac{A}{\varepsilon l} \tag{3.2}$$

where A is the absorbance of the iron in solution, ε is the molar absorptivity, C is the concentration of the iron, l is the path length of the cuvette. Figure 3.5 illustrates the setup for determining the absorbance of iron leached. A standard curve was then drawn to establish the linear relation between concentration and absorbance. The kinetics of leaching was then be studied.

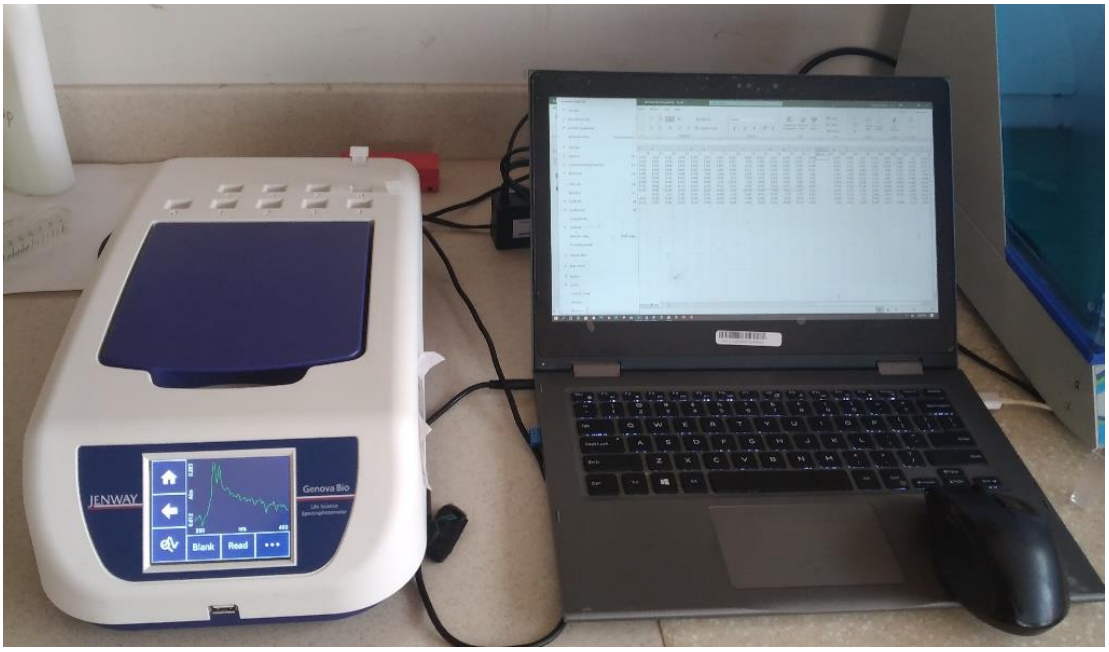

Figure 3.5: UV-Vis Spectroscopy Measurement Using JENWAY Device (Genova Bio Instrument).

3.3 kinetics of Leaching

Leaching was done using phosphoric and hydrochloric acid at a constant temperature of 94ºC. The Kinetic and the other of reactions was be studied. Leaching of iron oxide from clay sample can be explained with the shrinking core model [47], [48] :

$$aA_{Fluid} + bB_{particles} \rightarrow product$$

where a and b are the reaction stoichiometries.

When diffusion is dominant in the reaction through the product layer, there will be an integrated rate equation given as:

$$1 - \frac{2}{3}X - (1 - X)^{\frac{2}{3}} = K_d t$$

If chemical reaction on surface is the paramount reaction, the rate equation is:

$$1 - (1 - X)^{\frac{1}{3}} = k_c t$$

Where X is the fraction reacted, K_d is the kinetic parameter for diffusion control, t is the reaction time in minutes and K_c is the kinetic parameter for the chemical reaction control [49].

3.4 Kinetics Models of Iron release rates

The kinetics of iron leached was investigated using kinetics models as presented in Table 3.1. The kinetics models summarised in table 3.1 includes zero-order, first order, second order, and Higuchi model. A linear relation between iron [concentration] as a function of time satisfies a zeroth order if a linear graph with a regression coefficient, R^2 ~1 is obtain.

First-order kinetics was investigated when a plot of log [concentration] presents a linear graph with leaching time (Table 3.1). Similarly, the value of R^2 supports decisions through the goodness of fit. Moreover, a linear graph obtained from inverse of concentration versus time will represent a second-order model with respect to the R^2 value.

Higuchi model was also tested on the data from a plot of concentration versus square root of time ($t^{1/2}$) **[7].** The gradients from the kinetics model graphs represents the reaction coefficients/rate of reactions. The unit of k differs from one model to the other.

Table 3.1: Linear Relations of the Model Equation *[50]*.

Model	Equation	Equation Number
Zero-order	$C_t = \mathrm{C_{to}} + k_o t$	(3.4)
First-order	$lnC_t = lnC_{to} + k_1 t$	(3.5)
Second-order	$\frac{1}{C_t} = \frac{1}{C_{to}} + k_2 t$	(3.6)
Higuchi	$C_t = k_H t^{\frac{1}{2}}$	(3.7)

where C is the concentration of iron leached in solution at the time**,** t, C_{t_o} is the concentration of iron leached at t = 0, k_0, k_1, and k_2 are the reaction rate constants, and t is the reaction time.

3.5 Preparation of clay molds

Wooden planks were used for the mold for the test samples. Each rectangular mold was 10cm by 4cm by 2cm. A paste was formed by mixing the clay with about 1000mL of water. The perfect mix was then poured into the hollow rectangular portion in the wood and allowed to dry for about a week.

3.5.1 Flexural Strength

A three-point bend loading configuration will be used to estimate the flexural/bend strengths and fracture toughness values of the samples. The mechanical properties of the sample will also be determined. Five specimens were tested in each test and the average values were reported (Fig. 3.6a).

The flexural/bend strength, $\sigma bend$, was obtained from:

$$\sigma = \frac{3FL}{2bd^2}$$

where F is the fracture load, L is the span length of the specimen as previously presented in Figure 2.2, d is the height of the specimen, and b is the width of the specimen. The flexural modulus was also calculated as:

$$E = \frac{L^3 F}{4ba^3 \delta} \ (N/m^{-2}) \qquad (3.9)$$

where δ is the deflection of the beam when a load, F, is applied.

(a) (b)

Figure 3.6: Sample Preparation and Mechanical Testing: (a) Molded Test Samples for Flexural test: Compressive (b) Mechanical Testing of Specimens Using MTS Testing Machine.

CHAPTER FOUR

4.0 Result and Discussions

4.1. Material Characterization

4.1.1 Optical Morphologies of the Clay

SEM image (Fig. 4.1a) revealed a porous structure from the as-received clay ore obtain from the Savannah Region. The loosely and porous clay ore presented in Figure 4.1a enhance the comminution process, thereby breaking easily along the loosely structures. The optical morphologies from the USB microscope presented low magnified image that compares differences between the Volta clay and the Savannah Clay.

(a)

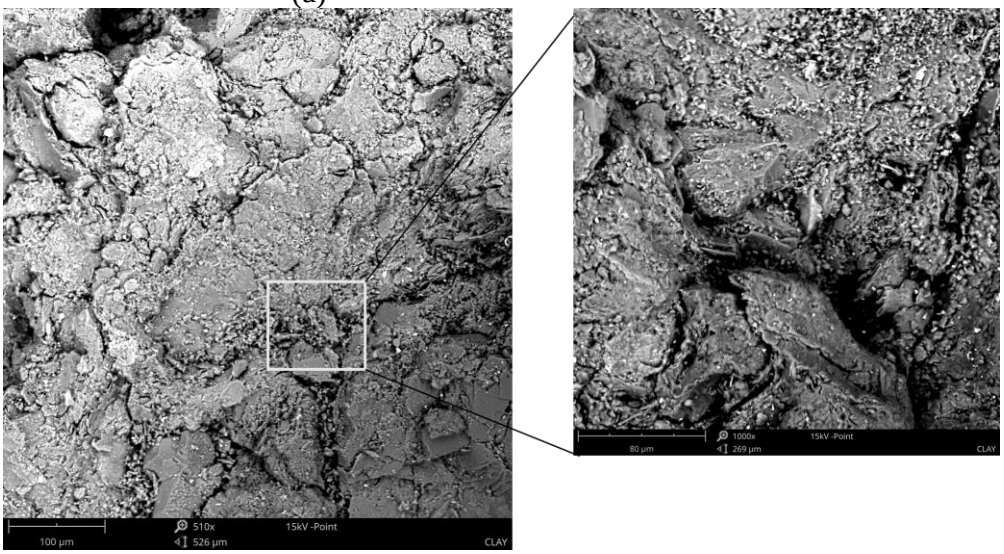

(b)

(c)

Figure 4.1: Morphological Analysis: Scanning Electron Microscopy Image of the Savanna Clay, (a) USB Microscope Image of Savannah Clay, (b) USB Image of Savannah Clay, and (c) USB Image of Volta Clay.

The images presented (Figs. 4.1b-c) above revealed the appearance of the two sources of clay ores. The clay sourced from the Savannah Region appeared grey, while the sample clay ore sourced from the Volta Region appeared reddish. The images indicate the presence of different compounds. Quartz particles were obviously seen on the micrographs as whitish particles with irregular shapes.

4.1.2 Elemental Composition of the Two Clay Ores

The X-Ray Fluorescence (XRF) analysis was used to determine the elements in the two different clay samples as seen in Table 4.1. The Major oxides (Table 4.2) were also determined from the clay samples using XRF.

Silica (SiO_2) a compound of the two most abundant elements in the earth's crust [1], [3] followed by Bauxite (Al_2O_3) [2], which is evident in Figure 4.1 and 4.2. Also, the different clays have iron contents which are <45%, therefore are categorized as grade I low-grade iron [30].

Table 4.1 Elemental composition of the Savannah and Volta clay

Elemental Component	Savannah Clay (mass%)	Volta Clay (mass%)
Mg	0.691	0.125
Al	13.1	10.5
Si	20.7	25.2
P	0.0175	0.0406
S	0.0032	0.0244
Cl	0.0029	0.0046
K	0.363	0.347
Ca	0.187	0.0438
Ti	0.49	0.551
V	0.0178	0.014
Mn	0.0291	0.0088
Fe	4.95	4.3
Co	0.0146	0.0097
Ni	0.0032	0.002
Cu	0.0045	0.0017
Zn	0.0086	0.0024
Ga	0.0027	0.0016
Rb	0.0028	0.0032
Sr	0.0033	0.002
Y	0.0018	0.0021
Sn	0.0015	0.0016
Au	0.0005	0.0005
Tl	0.0003	0.0004
Pb	0.0008	0.0016
O	59.3	58.9

Table 4.2 The oxide components present in both the Savannah Clay and the Volta clay

Oxide Component	**Savannah Clay (mass %)**	**Volta Clay (mass %)**
MgO	1.36	0.23
Al_2O_3	29.7	23.1
SiO_2	56.4	66
P_2O_5	0.0532	0.123
SO_3	0.0103	0.0739
K_2O	0.61	0.524
CaOh	0.363	0.085
TiO_2	1.1	1.24
V_2O_5	0.038	0.0347
Cr_2O_3	0.011	0.0136
MnO	0.0514	0.0144
Fe_2O_3	10.2	8.49
Co_2O_3	0.0379	0.0241
NiO	0.0059	0.0037
CuO	0.0079	0.0026
ZnO	0.0164	0.0042
Ga_2O_3	0.0053	0.0031
Rb_2O	0.0045	0.0049
SrO	0.006	0.0032
Y_2O_3	0.0032	0.0035
Nb_2O_5	0.0016	0.0056
SnO_2	0.0027	0.0033
HfO_2	0.0029	0.0032
Ta_2O_5	0.0029	0.0031
PbO	0.0014	0.0025
ThO_2	0.0012	0.0023
U_3O_8	0.0006	0.0011

Tables 4.1 and 4.2 indicate the presence of iron in both clay samples. From results in Table 4.2, there is 10 mass % Fe_2O_3 (hematite) of Savannah clay (grey coloured) whereas that of the Volta clay is about 8.49 in mass %. Literature suggests that hematite (Fe_2O_3) in clays gives them the red colour. It can be concluded that this hypothesis on iron-clay composition is not well understood. There is more to what literature has to say about this composition. Thus, colour should not be the basis of determining the material properties of clay.

4.1.3 X-Ray Diffraction (XRD)

X-ray diffraction technique primarily provides information for phase identification of a crystalline material. The graphs, Figure 4.2, and Figure 4.3, indicate intensity vs position (2θ). The sharp diffraction peaks in the graphs signify the crystallinity of the material being examined [51]. All XRD patterns as presented in Table 4.3 and 4.4 reflect the existence of silicate peaks; however, a new peak emerged in the Table 4.3 known as mmontmorillonite with a percentage of about 67.6%.

Figure 4.2 and 4.3 also shows the presence of quartz in them with percentages of 100 and 32.4, respectively. According to [51], quartz is one of the phases of SiO_2.

It can then be concluded that, the result obtained during the optical analysis of the two source clay ores is verified.

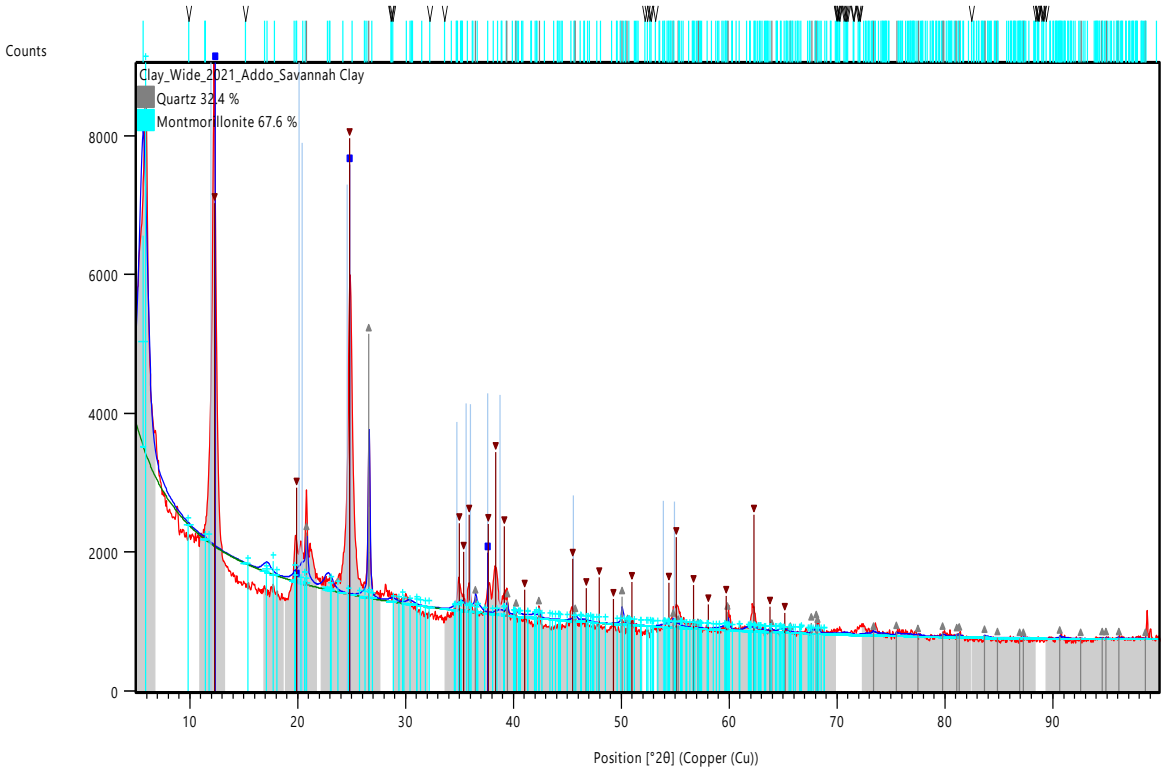

Figure 4.2: Results from XRD analysis of Savannah clay before leaching.

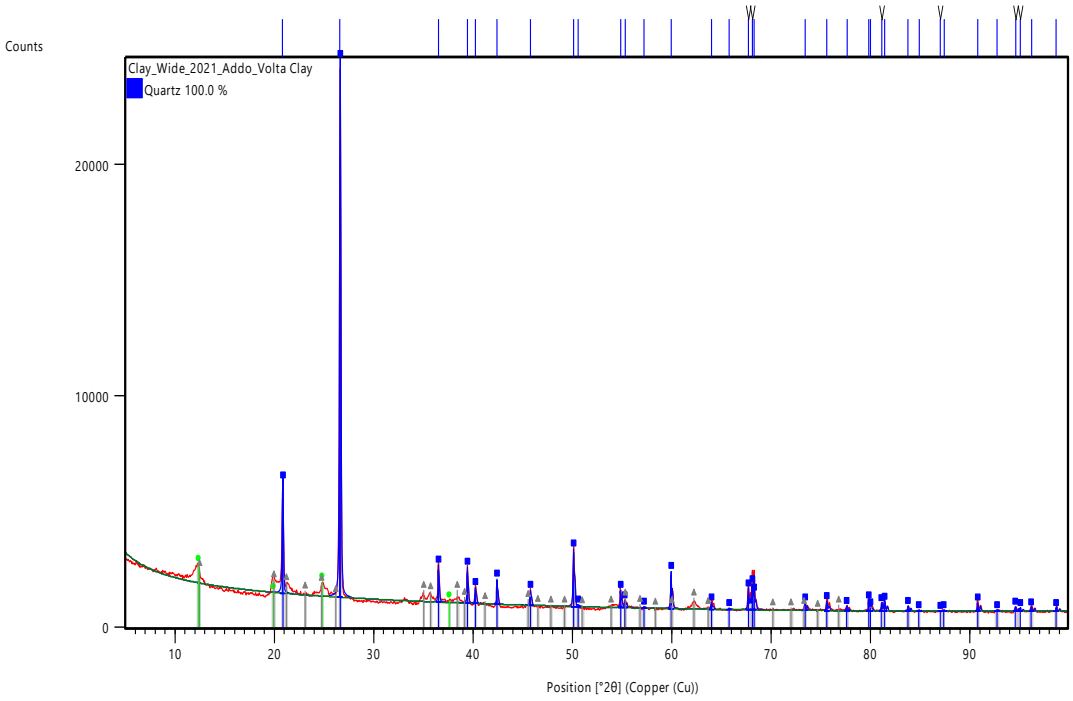

Figure 4.3: Results from XRD analysis of Volta clay before leaching.

Table 4.3 Pattern List from XRD for the Savannah Clay Before Leaching

Visible	Ref.Code	Score	Compound Name	Displ.[°2θ]	Scale Fac.	Chem. Formula
*	00-058-2002	18	Aluminum Silicate Hydroxide	0.000	0.873	Al2 Si2 O5 (O H)4
*	01-075-8320	17	Silicon Oxide	0.000	0.420	Si O2
*	00-058-2030	13	Aluminum Silicate Hydroxide	0.000	0.725	Al2 Si2 O5 (O H)4
*	98-016-1171	14	Montmorillonite	0.000	0.708	H1 Al2 Ca0.5 O12 Si4

Table 4.4: Pattern List from XRD for the Volta Clay Before Leaching

Visible	Ref.Code	Score	Compound Name	Displ.[°2θ]	Scale Fac.	Chem. Formula
*	01-070-3755	72	Silicon Oxide	0.000	0.942	Si O2
*	00-058-2002	14	Aluminum Silicate Hydroxide	0.000	0.033	Al2 Si2 O5 (O H)4
*	00-003-0052	15	Aluminum Silicate Hydroxide	0.000	0.025	Al2 O3 ·2 Si O2 ·2 H2 O

4.1.4 Chemical Analysis of the Clay Ores Using FTIR

The transmittance of iron in the clay sample as a function of wavenumber was determined with Fourier Transform Infrared Radiation Spectroscopy (FTIR). The analysis was

conducted to identify the functional groups and nature of bonds formed in the range of 500-4000 cm^{-1} **(Fig. 4.4a-c)**. **Figure 4.4c** presents the combined effect of spectra alignment of Savannah and volta clay samples. The FTIR spectrum (**Fig. 4.3c)** contains a peak at 3696.76 cm^{-1} indicating the presence of quartz due to SiOH and SiO_2**.** The peaks around 1112.47 cm^{-1} and 1032.53 cm^{-1} indicate the presence of kaolinite due to O-H bending band of Fe-OH.

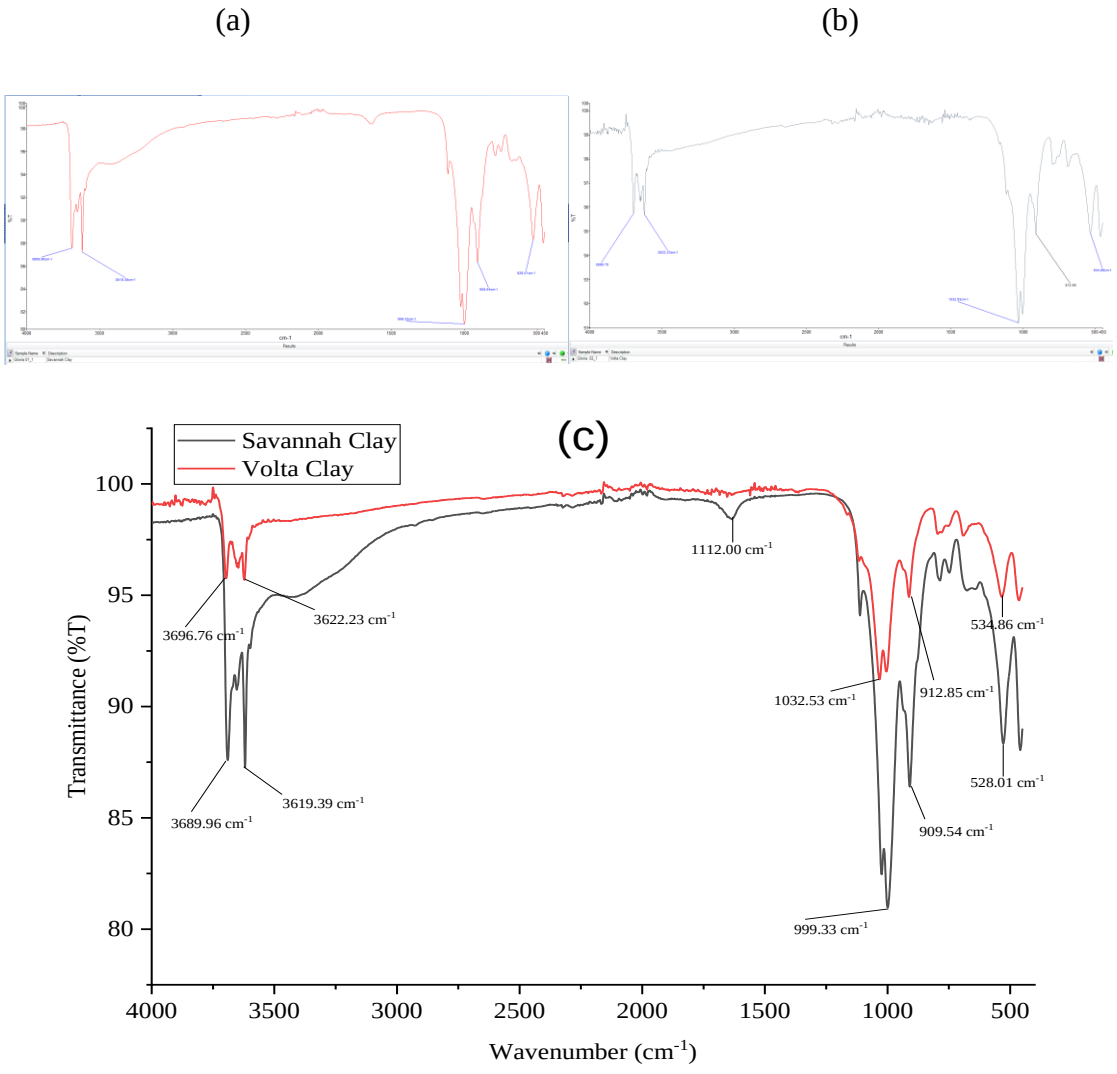

Figure 4.4: FTIR Spectroscopy Analysis of clay before leaching (a) Volta Clay (b) Savannah Clay (c) Combined Volta and Savannah Clay.

4.2 Standard Curve and Iron Concentration

From the Beer-Lambert, as shown earlier, the absorbance peak of iron oxide in solution was observed within the range of ~250-350 nm wavelength. Moreover, iron concentration versus absorbance for 1M, 2M and 3M is presented in the standard curves (Fig 4.7 – 4.10). Specifically, the absorption peaks occurred around 270 – 330nm (Fig 4.5 – Fig 4.6). A narrow absorption spectrum at 304 nm was observed in the UV-Vis spectra for 1.0M phosphoric acid. There was a shift in the absorption peaks with increasing leaching time. Meanwhile, the concentration of iron in solution continuous to increase with leaching time at a constant leaching temperature. However, the standard curves presented for Hydrochloric acid (Fig 4.9) revealed a common gradient. Similar results were observed for other acids used. This indicates the leaching process of iron with the different acids were determine by the materials properties and a diffusion governing mechanism.

(a)

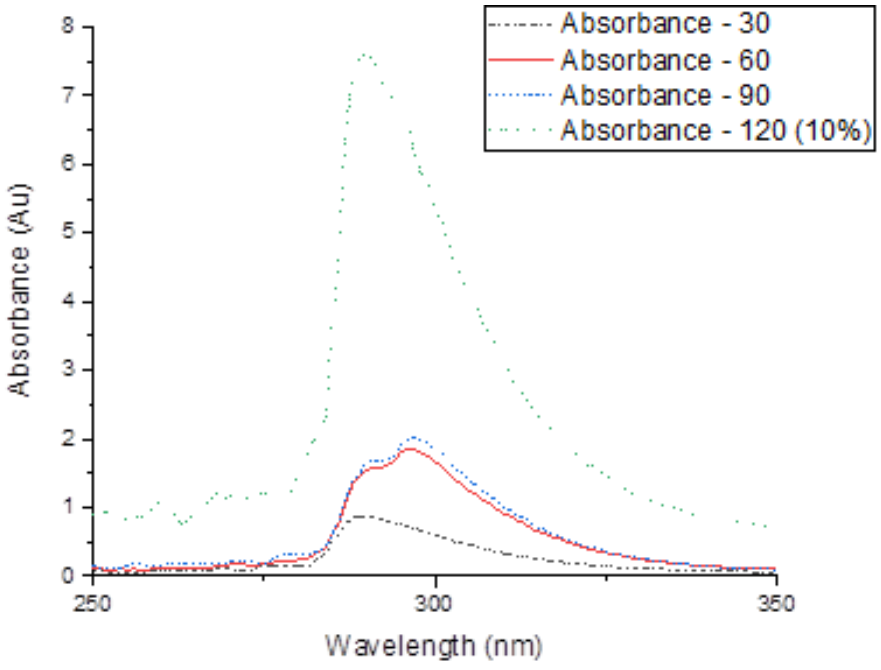

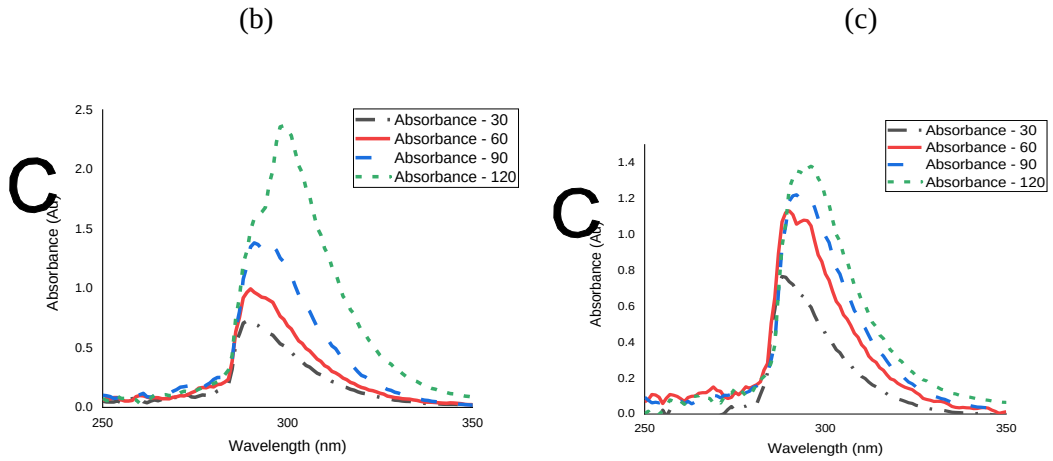

Figure 4.5: Effect of Leaching Time and Phosphoric Acid Concentration on the Iron Absorbance from the Volta Clay: (a) 1M, (b) 2M, and (c) 3M.

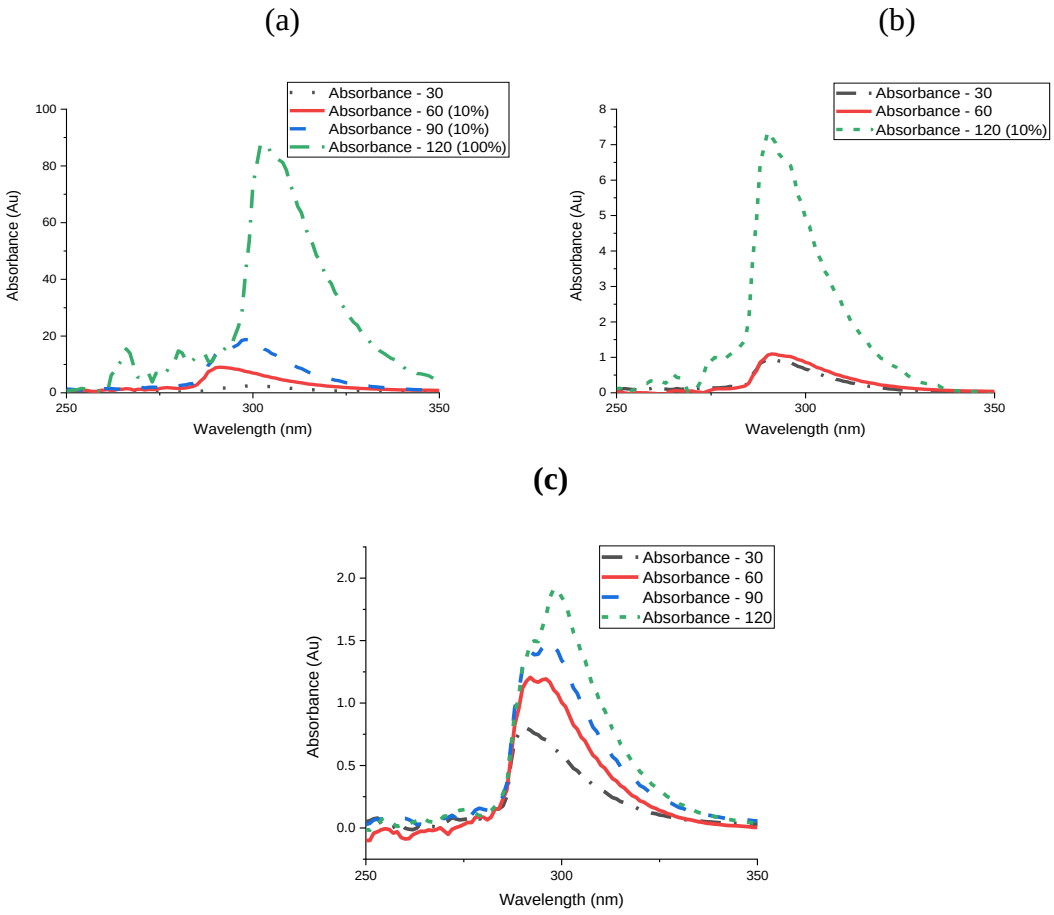

Figure 4.6: Effect of Leaching Time and Phosphoric Acid Concentration on the Iron Absorbance from the Savannah Clay: (a) 1M, (b) 2M, and (c) 3M.

Table 4.5: The absorbance and concentration of the iron oxide at 1.0M Phosphoric acid Solution of Volta Clay using Beer Lamberts equation

Leaching Duration (min)	Iron Concentration (L/mol ×10^{-3})	Absorbance (Au)
30	3.047	85
60	6.487	181
90	7.054	196.80
120	26.824	748.40

Table 4.6: The absorbance and concentration of the iron oxide at 2.0M phosphoric acid Solution of Volta Clay using Beer Lamberts equation

Leaching Duration (min)	Iron Concentration (L/mol ×10^{-3})	Absorbance (Au)
30	2.541	70.92
60	3.422	95.46
90	4.880	136.14
120	8.284	231.13

Table 4.7 The Absorbance and Concentration of the iron oxide at 3.0M Phosphoric acid Solution of Volta Clay Using Beer Lamberts equation.

Leaching Duration (min)	Iron Concentration (L/mol ×10^{-3})	Absorbance (Au)
30	2.657	74.14
60	3.957	110.4
90	4.325	120.68
120	4.887	136.36

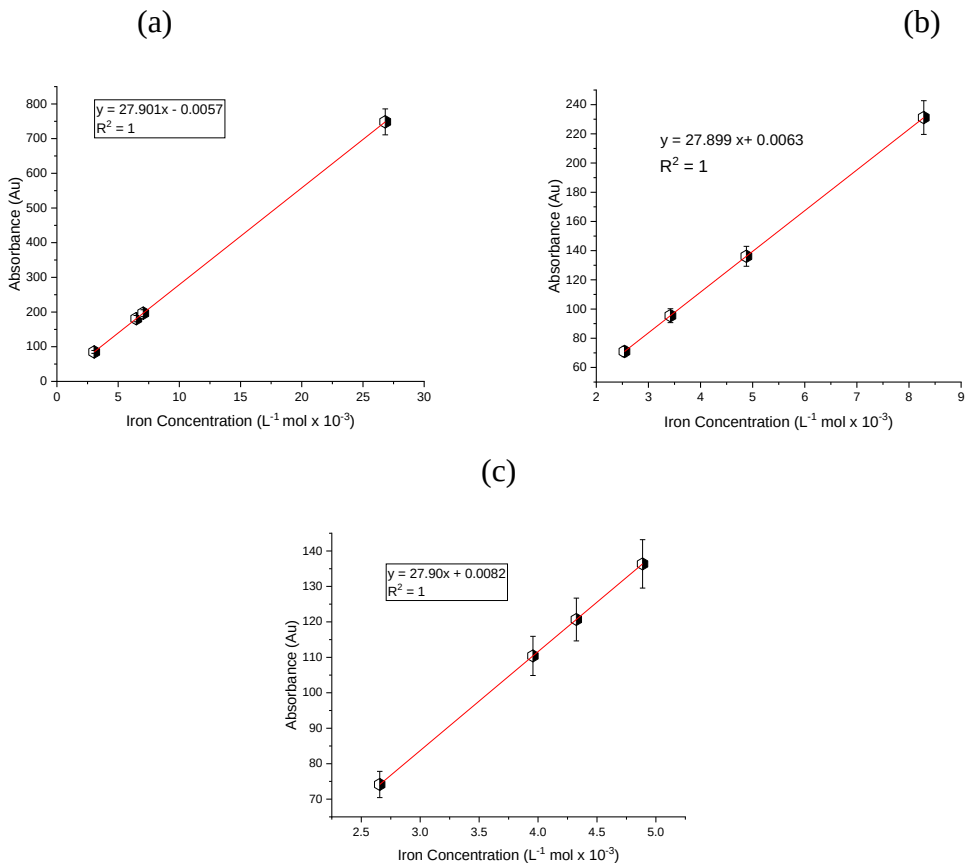

Figure 4.7: Standard Curve of Iron Leached from Volta Clay using Phosphoric Acid.

Table 4.8: The absorbance and concentration of the iron oxide at 1.0M Phosphoric acid Solution of Savannah clay using Beer Lamberts equation.

Leaching Duration (min)	Iron Concentration (L/mol ×10^{-3})	Absorbance (Au)
30	1.01	28.184
60	3.179	88.7
90	6.546	182.64
120	30.817	859.8

Table 4.9: The Absorbance and Concentration of the iron oxide at 2.0M Phosphoric Acid Solution of Savannah Clay using Beer Lamberts Equation.

Leaching Duration (min)	Iron Concentration (L/mol ×10^{-3})	Absorbance (Au)
30	3.301	92.10
60	3.837	107.04
90	6.039	168.48
120	25.297	705.8

Table 4.10: The Absorbance and Concentration of the iron oxide at 3.0M Phosphoric Acid Solution of Savannah Clay using Beer Lamberts Equation.

Leaching Duration (min)	Iron Concentration (L/mol ×10^{-3})	Absorbance (Au)
30	2.789	77.82
60	4.250	118.58
90	5.216	145.54
120	6.677	186.3

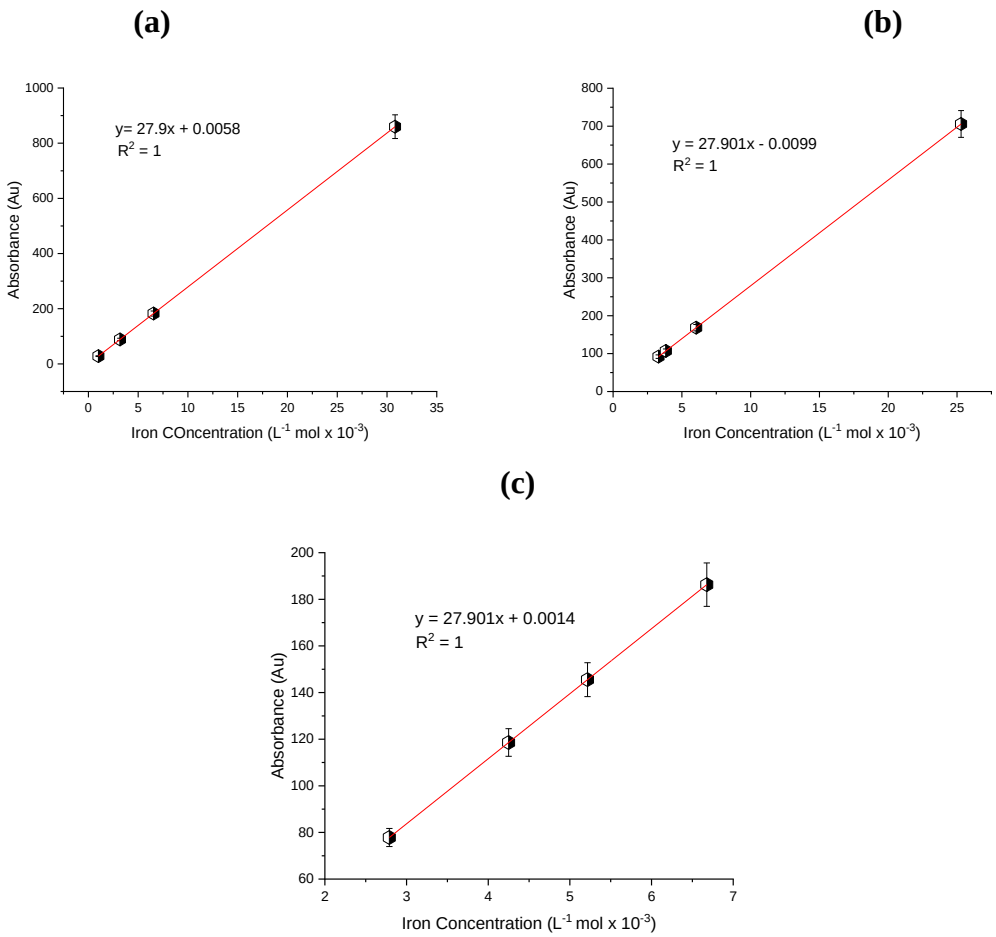

Figure 4.8: Standard Curve of Iron Leached from Savannah Clay using Phosphoric Acid.

Table 4.11: The Absorbance and Concentration of the Iron Oxide at 1.0M Hydrochloric Acid Solution of Volta Clay Using Beer Lamberts equation.

Leaching Duration (min)	Iron Concentration (L/mol ×10^{-3})	Absorbance (Au)
30	1.752	48.88
60	3.824	106.68
90	17.523	488.9
120	36.753	1025.4

Table 4.12: The Absorbance and Concentration of the Iron Oxide at 2.0M Hydrochloric Acid Solution of Volta Clay Using Beer Lamberts Equation.

Leaching Duration (min)	Iron Concentration (L/mol ×10^{-3})	Absorbance (Au)
30	3.571	99.64
60	3.719	103.76
90	7.290	203.40
120	17.505	488.4

Table 4.13: The Absorbance and Concentration of the Iron Oxide at 3.0M Hydrochloric Acid Solution of Volta Clay Using Beer Lamberts equation

Leaching Duration (min)	Iron Concentration (L/mol ×10^{-3})	Absorbance (Au)
30	2.028	56.58
60	3.457	96.44
90	3.563	99.4
120	7.556	210.8

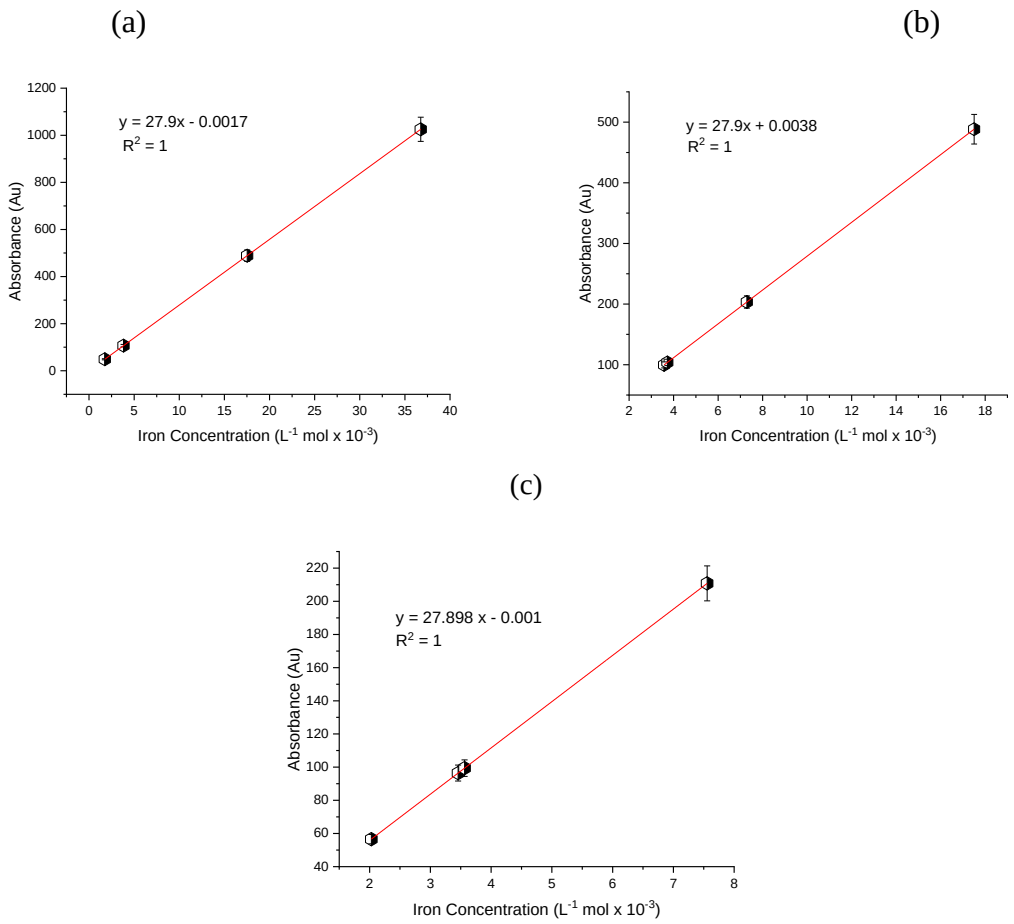

Figure 4.9: Standard Curve of Iron Leached from Volta Clay using Hydrochloric Acid.

Table 4.14: The Absorbance and Concentration of the iron oxide at 1.0M Hydrochloric Acid Solution of Savannah Clay Using Beer Lamberts Equation.

Leaching Duration (min)	Iron Concentration (L/mol ×10^{-3})	Absorbance (Au)
30	1.643	45.84
60	3.541	98.78
90	7.634	212.98
120	15.599	435.2

Table 4.15: The Absorbance and Concentration of the iron oxide at 2.0M Hydrochloric Acid Solution of Savannah Clay Using Beer Lamberts Equation.

Leaching Duration (min)	Iron Concentration (L/mol ×10^{-3})	Absorbance (Au)
30	2.857	79.72
60	5.089	141.98
90	7.351	205.1
120	8.129	226.8

Table 4.16: The absorbance and concentration of the iron oxide at 3.0M Hydrochloric Acid Solution of Savannah Clay Using Beer Lamberts equation

Leaching Duration (min)	Iron Concentration (L/mol ×10^{-3})	Absorbance (Au)
30	5.568	155.36
60	6.157	171.78
90	6.261	174.68
120	17.849	498

(a) (b)

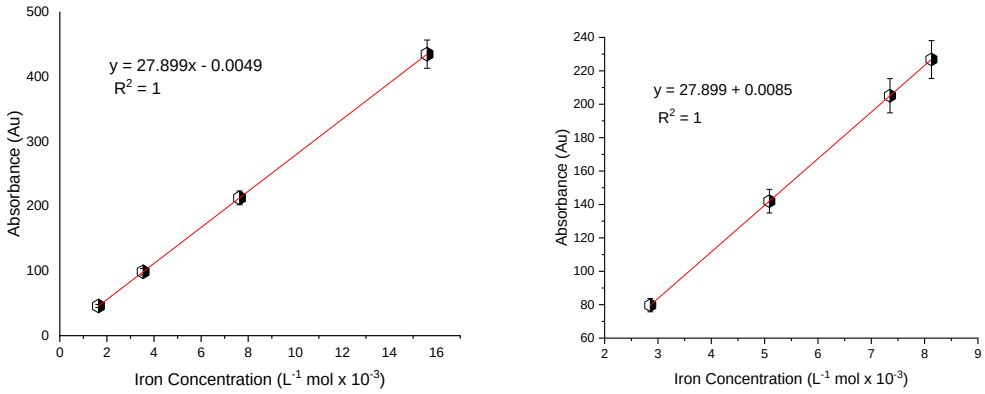

(c)

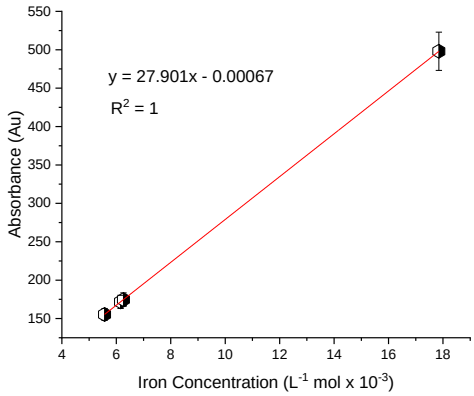

Figure 4.10: Standard Curve of Iron Leached from Savannah Clay using Hydrochloric Acid.

4.3 Kinetics of Iron Release

To better comprehend the kinetics of iron released, the zeroth-order, first order, second order, and Higuchi models were examined as discussed earlier. Calculations were performed to obtain the Concentrations (C), Ln (C), and inverse (C) for all concentrations of phosphoric and hydrochloric acid (1M, 2M, and 3M) for the two clay samples as indicated (**Table 4.18 – 4.29**). **Figure 4.11** shows the reaction kinetics of 1M phosphoric acid for the volta clay: the zeroth order, first – order, second – order, and Higuchi model.

The results (**Fig 4.11 – 4.19**) illustrate a graphical fitting of the data to the models. Moreover, the regression coefficient, R^2, was used to validate the goodness of fit to the model. For the Volta clay using phosphoric acid, 1M follows the second - order model with an R^2 of 0.924 in **Fig 4.11 (c)**; 2M also follows the Second model and obtained a regression value of 0.998 in **Fig 4.12 (c**); whereas 3M favours the Higuchi model with an R^2, 0.963 **(Fig.4.13 (a)).**

For the Volta clay using hydrochloric acid, 1M follows the first- order model with an R^2 of 0.975 in **Fig 4.17 (b)**; 2M follows the second-order model and obtained a regression value of 0.971 in **Fig 4.18(c**); whereas 3M favours the second-order as well with R^2 = 0.917 **(Fig.4.19 (c)).**

Table 4.17: Reaction Kinetics between 1M Phosphoric Acid and Iron Dissolution of the Volta Clay.

Time Interval (min)	**Square Root of time $(min)^{0.5}$**	**Iron Concentration (C) $(L^{-1}\ mol \times 10^{-3})$**	**Ln(C) $(L^{-1}\ mol \times 10^{-3})$**	$\frac{1}{(C)}$ **$(L/mol \times 10^{-3})^{-1}$**
30	5.477	3.047	1.114	0.328
60	7.746	6.487	1.87	0.154
90	9.847	7.054	1.954	0.142
120	10.954	26.824	3.289	0.037

Table 4.18: Reaction Kinetics between 2M Phosphoric Acid and Iron Dissolution of the Volta Clay.

Time Interval (min)	**Square Root of time $(min)^{0.5}$**	**Iron Concentration $(L^{-1}\ mol \times 10^{-3})$**	**Ln(C) $(L^{-1}\ mol \times 10^{-3})$**	$\frac{1}{(C)}$ **$(L/mol \times 10^{-3})^{-1}$**
30	5.477	2.541	0.933	0.394
60	7.746	3.422	1.230	0.292
90	9.847	4.880	1.585	0.205
120	10.954	8.284	2.114	0.121

Table 4.19: Reaction Kinetics between 3M Phosphoric Acid and Iron Dissolution of the Volta Clay.

Time Interval (min)	**Square Root of time $(min)^{0.5}$**	**Iron Concentration $(L^{-1}\ mol \times 10^{-3})$**	**Ln(C) $(L^{-1}\ mol \times 10^{-3})$**	$\frac{1}{(C)}$ **$(L/mol \times 10^{-3})^{-1}$**
30	5.477	2.657	0.977	0.376
60	7.746	3.957	1.375	0.253
90	9.847	4.325	1.464	0.231
120	10.954	4.887	1.587	0.205

Table 4.20: Reaction Kinetics between 1M Phosphoric Acid and Iron Dissolution of the Savannah Clay.

Time Interval (min)	**Square Root of time $(min)^{0.5}$**	**Iron Concentration (L^{-1} mol $\times 10^{-3}$)**	**Ln(C) (L^{-1} mol $\times 10^{-3}$)**	$\frac{\mathbf{1}}{(\boldsymbol{C})}$ **$(L/mol \times 10^{-3})^{-1}$**
30	5.477	1.01	0.001	0.99
60	7.746	3.179	1.157	0.315
90	9.847	6.546	1.879	0.153
120	10.954	30.817	3.428	0.032

Table 4.21: Reaction Kinetics between 2M Phosphoric Acid and Iron Dissolution of the Savannah Clay.

Time Interval (min)	**Square Root of time $(min)^{0.5}$**	**Iron Concentration (L^{-1} mol $\times 10^{-3}$)**	**Ln(C) (L^{-1} mol $\times 10^{-3}$)**	$\frac{\mathbf{1}}{(\boldsymbol{C})}$ **$(L/mol \times 10^{-3})^{-1}$**
30	5.477	3.301	1.194	0.303
60	7.746	3.837	1.345	0.261
90	9.847	6.039	1.798	0.166
120	10.954	25.297	3.231	0.04

Table 4.22: Reaction Kinetics between 3M Phosphoric Acid and Iron Dissolution of the Savannah Clay.

Time Interval (min)	**Square Root of time $(min)^{0.5}$**	**Iron Concentration (L^{-1} mol $\times 10^{-3}$)**	**Ln(C) (L^{-1} mol $\times 10^{-3}$)**	$\frac{\mathbf{1}}{(\boldsymbol{C})}$ **$(L/mol \times 10^{-3})^{-1}$**
30	5.477	2.789	1.026	0.359
60	7.746	4.250	1.447	0.235
90	9.847	5.216	1.652	0.192
120	10.954	6.677	1.899	0.15

Table 4.23: Reaction Kinetics between 1M Hydrochloric Acid and Iron Dissolution of the Volta Clay.

Time Interval (min)	**Square Root of time $(min)^{0.5}$**	**Iron Concentration (L^{-1} mol $\times 10^{-3}$)**	**Ln(C) (L^{-1} mol $\times 10^{-3}$)**	$\frac{\mathbf{1}}{(\boldsymbol{C})}$ **$(L/mol \times 10^{-3})^{-1}$**
30	5.477	1.752	0.561	0.571
60	7.746	3.824	1.341	0.262
90	9.847	17.523	2.864	0.057
120	10.954	36.753	3.604	0.027

Table 4.24: Reaction Kinetics between 2M Hydrochloric Acid and Iron Dissolution of the Volta Clay.

Time Interval (min)	**Square Root of time $(min)^{0.5}$**	**Iron Concentration (L^{-1} mol $\times 10^{-3}$)**	**Ln(C) (L^{-1} mol $\times 10^{-3}$)**	$\frac{\mathbf{1}}{(\boldsymbol{C})}$ **$(L/mol \times 10^{-3})^{-1}$**
30	5.477	3.571	1.273	0.28
60	7.746	3.719	1.313	0.269
90	9.847	7.290	1.987	0.137
120	10.954	17.505	2.862	0.057

Table 4.25: Reaction Kinetics between 3M Hydrochloric Acid and Iron Dissolution of the Volta Clay.

Time Interval (min)	**Square Root of time $(min)^{0.5}$**	**Iron Concentration (L^{-1} mol $\times 10^{-3}$)**	**Ln(C) (L^{-1} mol $\times 10^{-3}$)**	$\frac{\mathbf{1}}{(\boldsymbol{C})}$ **$(L/mol \times 10^{-3})^{-1}$**
30	5.477	2.028	0.707	0.493
60	7.746	3.457	1.24	0.289
90	9.847	3.563	1.271	0.281
120	10.954	7.556	2.022	0.132

Table 4.26: Reaction Kinetics between 1M Hydrochloric Acid and Iron Dissolution of the Savannah Clay.

Time Interval (min)	**Square Root of time $(min)^{0.5}$**	**Iron Concentration (L^{-1} mol $\times 10^{-3}$)**	**Ln(C) (L^{-1} mol $\times 10^{-3}$)**	$\frac{\mathbf{1}}{(\boldsymbol{C})}$ **$(L/mol \times 10^{-3})^{-1}$**
30	5.477	1.643	0.497	0.609
60	7.746	3.541	1.264	0.282
90	9.847	7.634	2.033	0.131
120	10.954	15.599	2.747	0.064

Table 4.27: Reaction Kinetics between 2M Hydrochloric Acid and Iron Dissolution of the Savannah Clay.

Time Interval (min)	**Square Root of time $(min)^{0.5}$**	**Iron Concentration (L^{-1} mol $\times 10^{-3}$)**	**Ln(C) (L^{-1} mol $\times 10^{-3}$)**	$\frac{\mathbf{1}}{(\boldsymbol{C})}$ **$(L/mol \times 10^{-3})^{-1}$**
30	5.477	2.857	1.05	0.35
60	7.746	5.089	1.627	0.197
90	9.847	7.351	1.995	0.136
120	10.954	8.129	2.095	0.123

Table 4.28: Reaction Kinetics between 3M Hydrochloric Acid and Iron Dissolution of the Savannah Clay.

Time Interval (min)	**Square Root of time $(min)^{0.5}$**	**Iron Concentration (L^{-1} mol $\times 10^{-3}$)**	**Ln(C) (L^{-1} mol $\times 10^{-3}$)**	$\frac{\mathbf{1}}{(\boldsymbol{C})}$ **$(L/mol \times 10^{-3})^{-1}$**
30	5.477	5.568	1.717	0.18
60	7.746	6.157	1.818	0.162
90	9.847	6.261	1.834	0.16
120	10.954	17.849	2.882	0.056

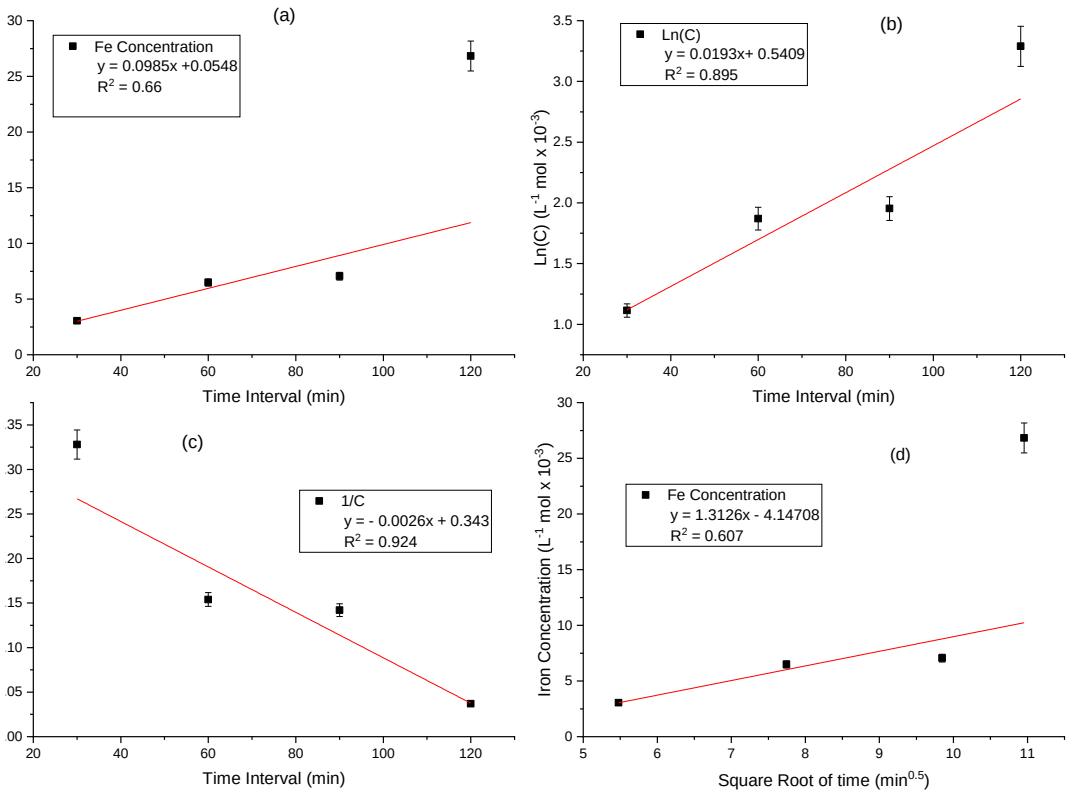

Figure 4.11: Kinetic Model Analysis on the Iron Release Rates for the Volta Clay using Phosphoric Acid at 1M (a) Zeroth- order (b) First – order (c) Second – order (d) Higuchi model.

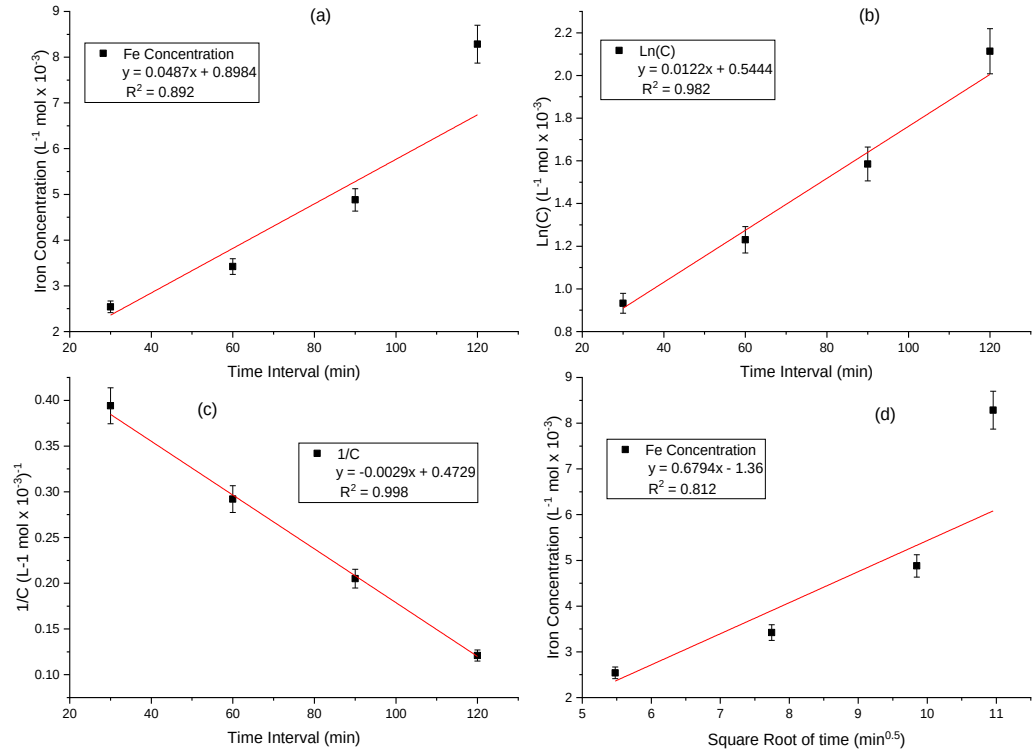

Figure 4.12: Kinetic Model Analysis on the Iron Release Rates for the Volta Clay using Phosphoric Acid at 2M (a) Zeroth- order (b) First – order (c) Second – order (d) Higuchi model.

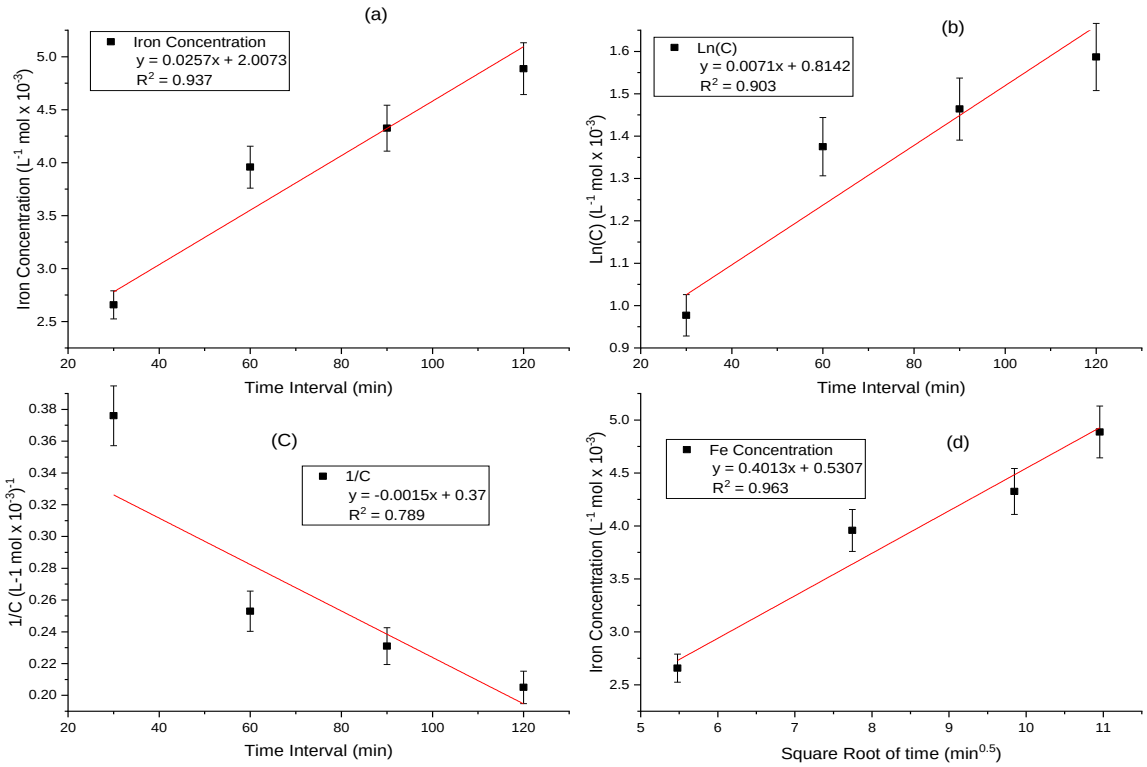

Figure 4.13: Kinetic Model Analysis on the Iron Release Rates for the Volta Clay using Phosphoric Acid at 3M (a) Zeroth- order (b) First – order (c) Second – order (d) Higuchi model.

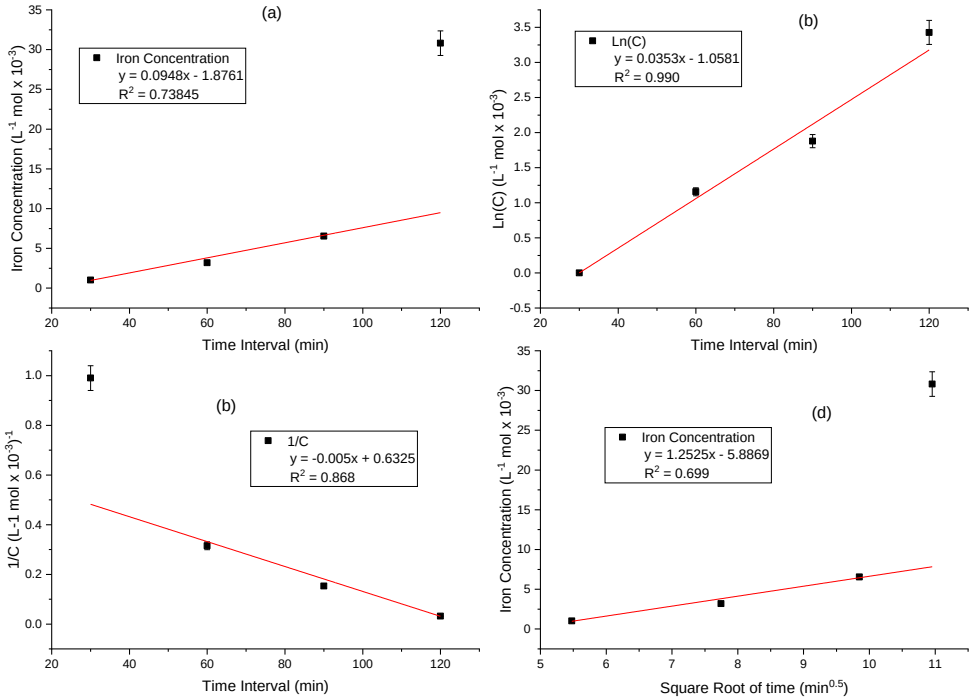

Figure 4.14: Kinetic Model Analysis on the Iron Release Rates for the Savannah Clay using Phosphoric Acid at 1M (a) Zeroth- order (b) First – order (c) Second – order (d) Higuchi model.

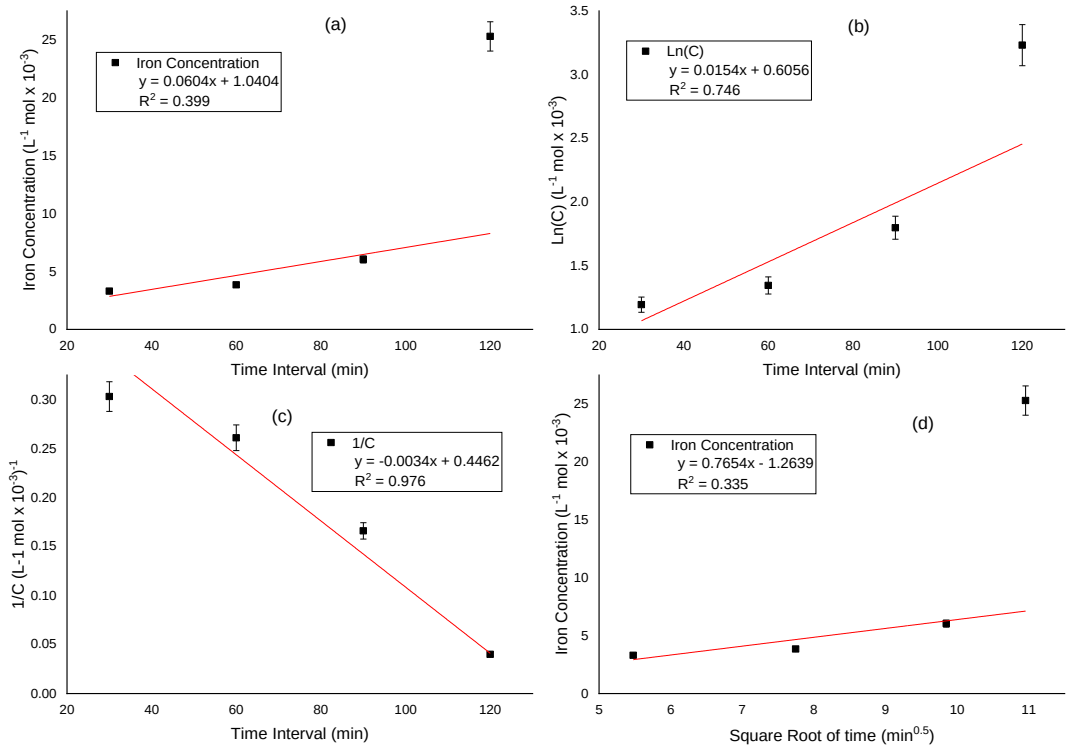

Figure 4.15: Kinetic Model Analysis on the Iron Release Rates for the Savannah Clay using Phosphoric Acid at 2M (a) Zeroth- order (b) First – order (c) Second – order (d) Higuchi model.

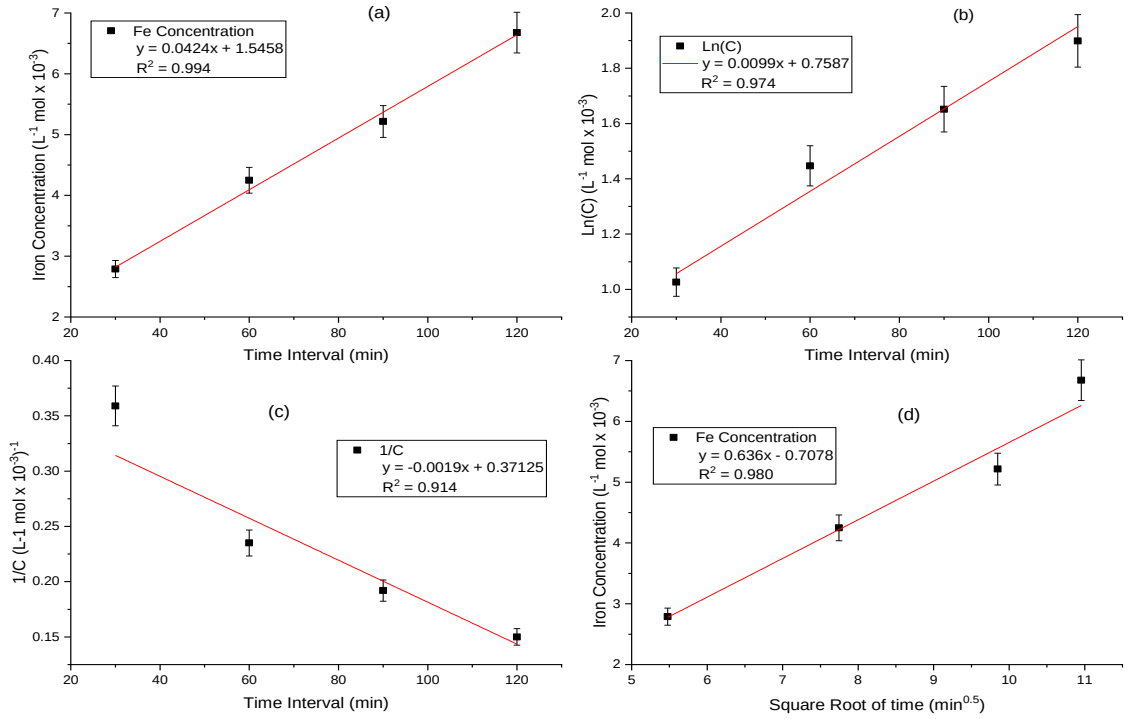

Figure 4.16: Kinetic Model Analysis on the Iron Release Rates for the Savannah Clay using Phosphoric Acid at 3M (a) Zeroth- order (b) First – order (c) Second – order (d) Higuchi model.

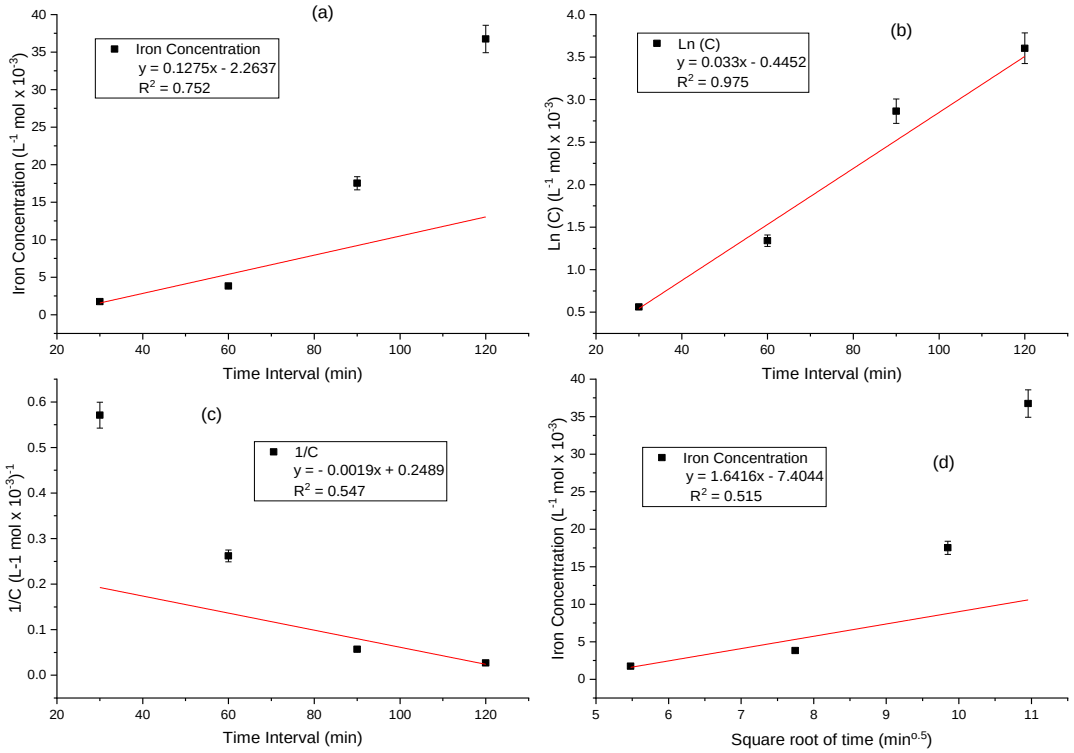

Figure 4.17: Kinetic Model Analysis on the Iron Release Rates for the Volta Clay using Hydrochloric Acid at 1M (a) Zeroth- order (b) First – order (c) Second – order (d) Higuchi model.

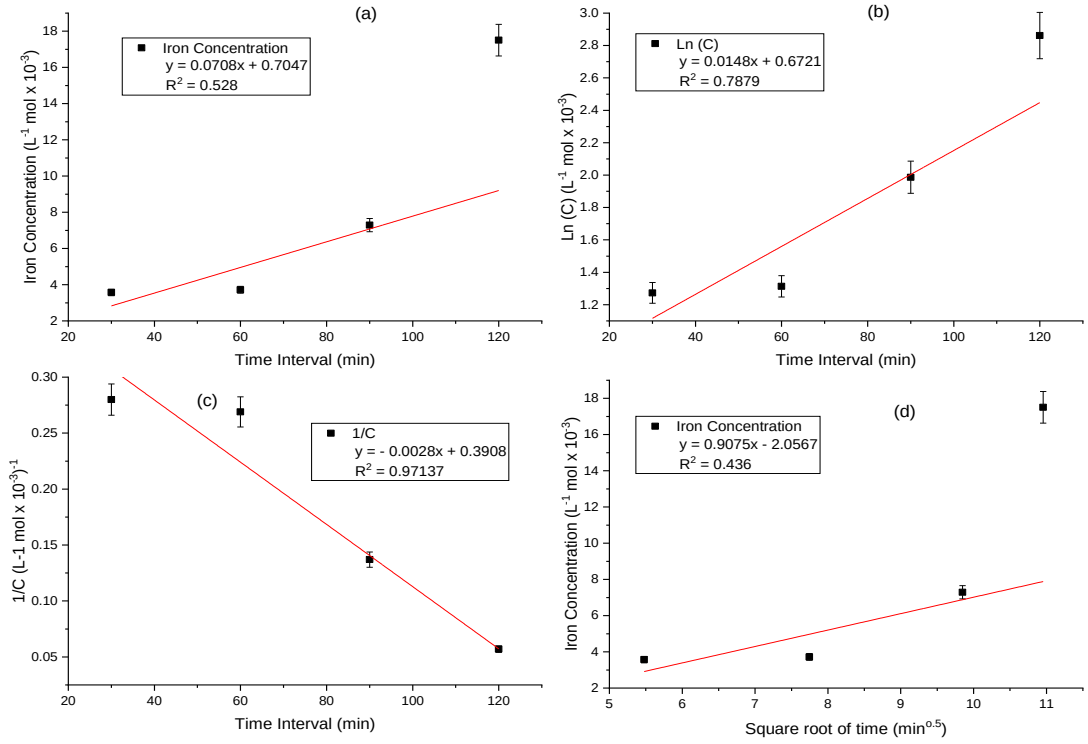

Figure 4.18: Kinetic Model Analysis on the Iron Release Rates for the Volta Clay using Hydrochloric Acid at 2M (a) Zeroth- order (b) First – order (c) Second – order (d) Higuchi model.

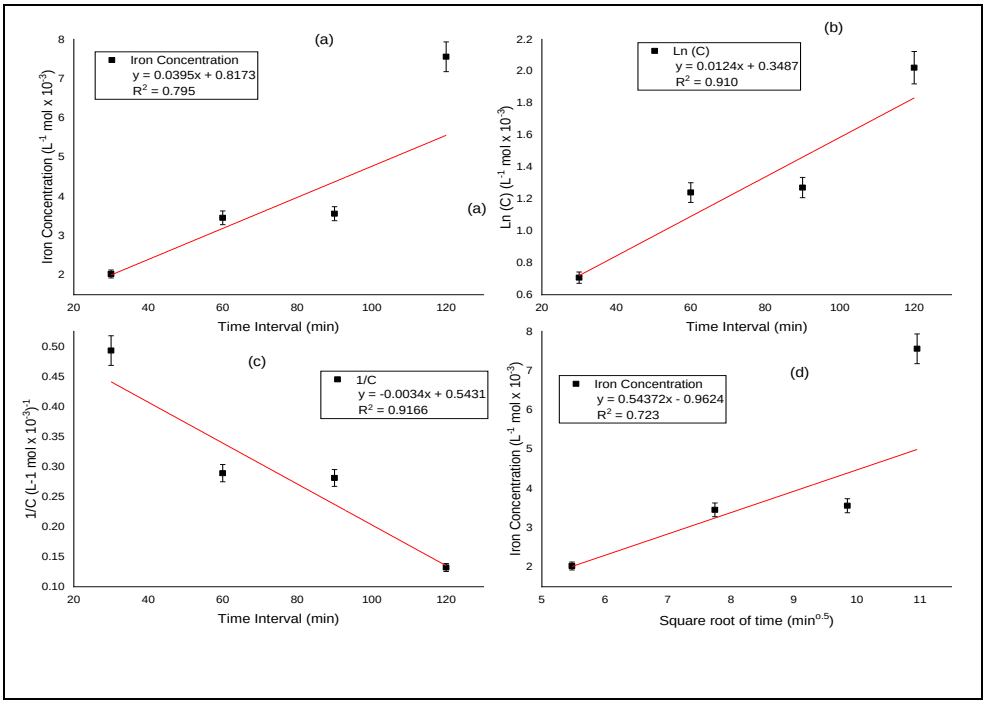

Figure 4.19: Kinetic Model Analysis on the Iron Release Rates for the Volta Clay using Hydrochloric Acid at 3M (a) Zeroth- order (b) First – order (c) Second – order (d) Higuchi model.

4.4 Mechanical Characterisation

Summary of results from the 3-point bend test of the Volta and Savannah clay samples are listed below.

Table 4.29: Results from 3-point bend test for Volta Clay

Characteristics	Sample 1	Sample 2	Sample 3	Sample 4	Sample 5	Average
Flexural Strength (kPa)	739.3	675	642.8	900	428	**677**
Load at fracture (N)	69	63	60	84	40	**63.2**
Flexural Strain (mm/mm)	0.00132	0.0027	0.00242	0.00339	0.00126	**0.00222**
Flexural Modulus (MPa)	14.9	6.6	7.1	7.1	9.1	**8.96**

Table 4.30: Results from 3-point bend test for Savannah Clay

Characteristics	Sample 1	Sample 2	Sample 3	Sample 4	Sample 5	Average
Flexural Strength (kPa)	2175	2057	2207	2282	3106	**2365.4**
Load at fracture (N)	203	192	206	213	193	**201.4**
Flexural Strain (mm/mm)	0.00245	0.0036	0.0012	0.00214	0.0064	**0.00316**
Flexural Modulus (MPa)	23.7	16.3	49	28	8.6	**25.12**

The flexural strength as well as its modulus as seen in Table 4.30 for Savannah clay is higher than that of the volta clay (Table 4.29). It can be concluded that the Savannah clay will be able to withstand a lot more force than the Volta clay. Hence, possess some ductile properties.

The summary results of the Compression tests are listed below as well.

Table 4.31: Results from the compression test for Volta Clay

Characteristics	Sample 1	Sample 2	Sample 3	Sample 4	Sample 5	Average
Compressive Strength (kPa)	700.6	637.4	700.6	637.4	635.4	**662.3**
Peak Load (N)	344	313	344	313	312	**325.2**
Flexural Strain (mm/mm)	0.04	0.06	0.04	0.06	0.09	**0.06**
Flexural Modulus (MPa)	39.9	64.9	4.8	4.6	31.2	**29.1**

Table 4.32: Results from the compression test for Savannah Clay

Characteristics	Sample 1	Sample 2	Sample 3	Sample 4	Sample 5	Average
Compressive Strength (kPa)	551.9	543.8	1042.8	598.8	551.9	**657.84**
Peak Load (N)	271	267	512	294	271	**323**
Flexural Strain (mm/mm)	0.16	0.07	0.09	0.05	0.16	**0.106**
Flexural Modulus (MPa)	51.4	34.5	66.4	22.6	51.4	**45.3**

For the 3-point bend test, the volta clay (**Table 4.31**) has its compressive strength and Flexural modulus to be greater than that of savannah, **Table 4.32**. Literature proves that concrete compressive strength for general construction varies from 15MPa t0 30 MPa; although higher in commercial and industrial structures. Thus, both clays are good materials to be used for small scale building projects.

CHAPTER 5

5.0 Conclusion and Recommendation for Future work

5.1 Conclusion

In this paper, iron oxide was investigated from two sourced clay: Volta and Savannah clay; by leaching with phosphoric and hydrochloric acid. The synthesized iron oxide was analysed by FTIR, UV-Vis Spectroscopy, XRD and XRF.

Conducting XRF analysis provided information on the elemental components of the two different clays. The result revealed the presence of important elements such as Fe, O and major oxides such as Fe_2O_3 (hematite). An indication of the presence of Fe in the clays allowed for further synthesis.

Leaching of iron with phosphoric and hydrochloric acid showed that as the Molarity of acid increases, the diffusion of Fe from the clay sample increases.

UV-Vis was carried out to verify the formation of iron oxide in the solution. An absorbance of about 280 - 450 nm wavelength was observed which agrees with literature to produce the magnetic iron oxide nanoparticles.

5.2 Recommendation for future work

Further analysis could be conducted to confirm the formation of Iron oxide Nanoparticles (IONPs) which will then be implemented for biomedical applications. Also safer ways of precipitating these IONPs from the filtrate should be considered. Transmission Electron Microscopy (TEM) could be used to investigate the IONPs particle size and morphology.

The IONPs could be functionalized with molecular recognition unit for an *in-vitro* experiment. Future work could be done to investigate the effect of the IONPs particle size.

References

[1] J. Dixon, "Roles of clays in soils," *Applied Clay Science,* vol. 5, no. 5-6, pp. 489-503, 1991.

[2] N. Ural, "The Importance of Clay in Geotechnical Engineering," in *Current Topics in the Utilization of Clay in Industrial and Medical Applications*, 2018, pp. 84-101.

[3] R. E. Grim and Kodama, "Article," Encyclopedia Britannica, 20 February 2014. [Online]. Available: https://www.britannica.com/science/clay-mineral. [Accessed 26 March 2021].

[4] E. N. Njoka, O. Ombaka, J. M. Gichumbi, D. I. Kibaara and O. M. Nderi, "Characterisation of clay from Tharaka-Nithi county in Kenya for industrial and agricultural applications," *African Journal of Environmental Science and Technology,* vol. 9, no. 3, pp. 228-243, 2015.

[5] J. W. Stucki, "Chapter 8 Properties and Behaviour of Iron in Clay Minerals," *Developments in CLay Science,* vol. 1, pp. 423-475, 2006.

[6] Y. Lu, W. Wang, J. Xu, J. Ding, Q. Wang and A. Wang, "Solid-phase oxalic acid leaching of natural red palygorskite-rich clay: A solvent-free way to change color and properties," *Applied Clay Science,* vol. 198, 2020.

[7] M. Jung, C. Mertens, E. Tomat and B. Brune, " Iron as a Central Player and Promising Target in Cancer Progression.," *International journal of molecular sciences,* vol. 20, no. 2, p. 273, 2019.

[8] National Institutes of Health, "Understanding Cancer," 2007. [Online]. Available: https://www.ncbi.nlm.nih.gov/books/NBK20362/. [Accessed 28 March 2021].

[9] K. H. Bae, J. H. Chung and G. T. Park, "Nanomaterials for Cancer Therapy and Imaging," *Molecules and Cells,* vol. 31, pp. 295 - 302, 2011.

[10] World Health Organization, "Cardiovascular diseases," WHO, [Online]. Available: https://www.who.int/health-topics/cardiovascular-diseases#tab=tab_1. [Accessed 28 March 2021].

[11] The World Health Organization, "Cancer," World Health Organization, 2021. [Online]. Available: https://www.who.int/news-room/fact-sheets/detail/cancer. [Accessed 21 March 2021].

[1 B. Khullar and S. Iqbal, "Size Matters: Nanoparticles in Cancer Therapy,"
2] *Current Science,* vol. 111, no. 10, pp. 1583 - 1584, 2016.

[1 Cancer.Net, "Navigating cancer care," 2019. [Online]. Available:
3] https://www.cancer.net/navigating-cancer-care/how-cancer-treated/chemotherapy/side-effects-chemotherapy. [Accessed 28 March 2021].

[1 Cancer.Net, "Understanding Radiation Therapy," 2020. [Online]. Available:
4] https://www.cancer.net/navigating-cancer-care/how-cancer-treated/radiation-therapy/understanding-radiation-therapy. [Accessed 29 March 2021].

[1 D. L. Miglioretti, J. Lange, J. J. Broek, C. I. Lee, K. Kerlikowske, J. J.
5] Fenton, J. Melnikow, H. J. Koning and R. A. Hubbard, "Radiation-Induced Breast Cancer Incidence and Mortality from Digital Mammography Screening: A Modeling Study," *Ann Intern Med.,* vol. 164, no. 4, pp. 205-214, 2016.

[1 S. V. Torti and F. M. Torti, "Iron and Cancer: more ore to be mined," *Nat*
6] *Rev Cancer,* vol. 13, no. 5, pp. 342-355, 2013.

[1 R. A. Revia and M. Zhang, "Magnetite nanoparticles for cancer diagnosis,
7] treatment, and treatment monitoring: recent advances," *Materials today,* vol. 19, no. 3, pp. 157-168, 2016.

[1 D. J. Obayemi, S. Dozie-Nwachukwu, Y. Danyuo, O. S. Odusanya, N.
8] Anuku, K. Malatesta and W. O. Soboyejo, "Biosynthesis and the conjugation of magnetite nanoparticles with luteinizing hormone releasing hormone(LHRH)," *Mater Sci C MAter Bio Appl.,* vol. 46, pp. 482 - 496, 2015.

[1 Y. Danyo, J. D. Obayemi, S. Dozie-Nwachukwu, C. J. Ani, S. O.
9] Odusanaya, Y. Oni, N. Anuku, K. Malatesta and W. O. Soboyejo, "Prodigiosin release from an implantable biomedical device: kinetics of localized cancer drug disease," *Material Science and Engineering,* vol. 42, pp. 734 - 745, 2004.

[2 National Cancer Institute, "About Cancer," National Cancer Institute, 2018.
0] [Online]. Available: https://www.cancer.gov/about-cancer/treatment/types/radiation-therapy/side-effects. [Accessed 26 March 2021].

[2 A. Amarkai, J. Efavi and E. K. Tiburu, "Biosynthesis of Magnetite iron oxide
1] Nanoparticles and its potential Application for Cancer Treatmtnt," vol. 10, no. 2, pp. 1-15, 2018.

[2 M. B. Fakoya, "Natural Resource, Value added and Economic Growth:
2] Empirical Analysis from Selected African Countries," *Journal of Human Ecology,* vol. 48, no. 2, pp. 227-233, 2014.

[2 O. C. Farokhzad and R. Langer, "Impact of nanotechnology on drug
3] delivery," *National Library of Medicine,* vol. 3, no. 1, pp. 16 - 20, 2009.

[2 Y. Kelly and M. Kim, "Nanotechnology platforms and physiological
4] challenges for cancer therapeutics," *Nanomedicine: Nanotechnology, Biology and Medicine,* vol. 3, no. 2, pp. 103-110, 2007.

[2 National Nanotechnnology Initiative, "Nano 101," National
5] Nanotechnnology Initiative, [Online]. Available: https://www.nano.gov/you/nanotechnology-benefits#:~:text=Nanotechnology%20is%20helping%20to%20considerably,environmental%20science%2C%20among%20many%20others.. [Accessed 27 March 2021].

[2 R. Service, "Nanotechnology Takes Aim at Cancer," *Science,* vol. 310, no.
6] 5751, pp. 1132-2234, 2005.

[2 U.S. Geological Survey, "Environmental Characteristics of Clays and Clay
7] Mineral Deposits," 1999. [Online]. Available: https://pubs.usgs.gov/info/clays/#:~:text=Clays%20and%20clay%20minerals%20are,and%20weathering%20of%20crystal%20tuff. [Accessed 30 March 2021].

[2 R. B. Asamoah, E. Nyankson, E. Annan, B. Agyei-Tuffour, J. K. Efavi, K.
8] Kan-Dapaah, V. A. Apalangya, L. W. Damoah, D. Dodoo-Arhin, E. K. Tiburu, S. K. Kwofie, B. Onwona-Agyeman and A. Yaya, "Industrial Applications of Clay Materials from Ghana - A Review," *Oriental Journal of Chemistry,* vol. 34, no. 4, p. Doi:10.13005/ojc/340403., 2018.

[2 A. Kay, "Iron: Types of Iron Ore," 28 June 2018. [Online]. Available:
9] https://investingnews.com/daily/resource-investing/base-metals-investing/iron-investing/types-of-iron-ore-hematite-vs-magnetite/. [Accessed 30 March 2021].

[3 Y. Chokshi, M. A. Limaye, S. K. Dutta and D. R. Lodhari, "Mineralogical
0] Studies of Low-Grade Iron form Jharkhand - Orissa Region, India," *Transactions of the Indian Institute of Metals,* pp. 151-155.Doi:org/10.1007/s12666-015-0740-4, 2016.

[3 U.S. DEPARTMENT OF ENERGY, "Forms of Iron Minerals, Ores, and Rocks,"
1] *Energy and Environmental Profile of the U.S. Mining Industry,* vol. 24, pp. 1-13, 1992.

[3 Britannica, "Article: Ores," 2021. [Online]. Available:
2] https://www.britannica.com/technology/iron-processing/Iron-making. [Accessed 30 March 2021].

[3 J. Park, J. Yeojin, P. Kusumah, J. Lee, K. Kwon and C. K. Lee, "Application
3] of Ionic Liquids in Hydrometallurgy," *International Journal of Molecular Sciences,* vol. 15, pp. 15320-15343; Doi:10.3390/ijms150915320, 2014.

[3 D. S. Smith, "Hydrometallurgy," pp. 1-29, 2001.
4]

[3 CGIS, May 2019. [Online]. Available: https://cgis.ca/article-
5] hydrometallurgy-valves/. [Accessed 18 April 2021].

[3 International Organization for Standardization, Plastics - Determination of
6] flexural properties, https://www.iso.org/obp/ui/#iso:std:iso:178:ed-6:v1:en:fig:1, 2019.

[3 O. Ombaka, "Characterization and classification of clay minerals for
7] potential applications in Rugi Ward, Kenya," *African Journal of Environmental Science and Technology,* vol. 10, no. 11, pp. 415-431, 2016.

[3 V. Vishwakarma and S. Uthaman, "Environmental impact of sustainable
8] green concrete," *Smart Nanoconcretes and Cement-Based Materials,* pp. 24-255, Doi:10.1016/B978-0-12-817854-6.00009-X, 2020.

[3 J. M. Guthrie, "Overview of X-ray Fluorescence," 2012. [Online]. Available:
9] https://archaeometry.missouri.edu/xrf_overview.html. [Accessed 29 March 2021].

[4 A. Barhoum, L. M. Garcia-Betancourt, H. Rahier and G. V. Assche,
0] "Physicochemical characterization of nanomaterials: polymorph, composition, wettability, and thermal stability," *Emerging Applications of Nanoparticles and Architecture Nanostructures,* pp. 255-278, Doi:10.1016/B978-0-323-51254-1.00009-9, 2018.

[4 Intertek, "Fourier Transform Infrared Spectroscopy (FTIR) analysis," 2020.
1] [Online]. Available: https://www.intertek.com/analysis/ftir/. [Accessed 29 March 2021].

[4 S. Petit and J. Madejova, "Fourier Transform Infrared Spectroscopy,"
2] *Development in Clay Science,* vol. 5, pp. 213-231, Doi:10.1016/B978-0-08-098259-5.00009-3., 2013.

[4 F. S. Rocha, A. J. Gomes, C. N. Lunardi, S. Kaliaguine and G. S. Patience,
3] "Experimental methods in chemical engineering: Ultraviolet visible spectroscopy—UV-Vis," *The Canadian Journal of Chemical Engineering,* vol. 96, no. 12, pp. 2512-2517, Doi: 10.1002/cjce.23344., 2018.

[4 R. A. Hemandez, L. Garcia, L. E. Cruz and L. Martinez, "Iron removal from
4] a kaolinitic clay by leaching to obtain high whiteness index," *Third Congress on Materials Science and Engineering ,* vol. 45, pp. Doi:10.1088/1757-899X/45/1/012002, 2012.

[4 R. A. Hemandez-Hemandez, F. Legorreta-Gracia, L. E. Hemandez-Cruz, E.
5] A. Chavez-Urbiola and E. Salinas-Rodriguez, "Kinetics of Iron Leaching from a Kaolinitic clay, using Phosphoric acid," *Minerals,* pp. 1-8, 2016.

[4 A. Shafiee, E. Ghadiri, J. Kassis, D. Williams and A. Atala, "Energy Band
6] Gap Investigation of Biomaterials: A Comprehensive Material Aproach for Bicompatibility of Medical Electronic Devices," *PMCID,* vol. 11, no. 1, p. 105. Doi: 10.3390/mi11010105, 2020.

[4 S. I. Patterson, S. H. Murray and H. H. Lefond, "Industrial Minerals and
7] Rocks," *AIME New York,NY,USA, 1983,* 1983.

[4 J. D. L and D. F. S. S. K. Kohl, "Demonstration of Absorbance using Digital
8] Color Image Analysis and colored Solutions," *Chem Educ,* vol. 83, no. 4, pp. 644-646, 2016.

[4 Yuliusman, R. A. Amiliana, P. T. Wulandari, M. Huda and F. A.
9] Kusumadewi, "Process optimization and leaching kinetics of zinc and manganese metals from zinc-carbon and alkaline spent batteries using citric acid reagent," *Material Science and Engineering,* vol. 333, pp. Doi:10.1088/1757-899X/333/1/012037, 2017.

[5 H. K. Shaikh, R. V. Kshirsagar and S. G. Patil, "Mathematical models for
0] grug release characterization: A review," *World Journal of pharmacy and pharmaceutical sciences. ,* vol. 4, no. 4, pp. 324-338., 2017.

[5 S. A. Speakman, "Introduction to X-Ray Powder Diffraction Data Analysis,"
1] [Online]. Available: http://prism.mit.edu/xray/introduction%20to%20xrpd%20data%20analysis.pdf. [Accessed 26 April 2021].

[5
2]

APPENDIX A

Clay/Sample No.	Wet-Dry Shrinkage (%)	Moisture Content (%)	Plasticity (Rule of Thumb)	Water of Plasticity (By Weight)	Colour of Raw Clay
Western Region					
Esiama (ESA)					
ESA1	2	10.54	Low	Low	
ESA2	3.28	21.11	Medium	High	
ESA3	4.52	25	Medium	High	
ESA4	2.83	16.19	Medium	High	
Nkroful(NKA)					
NKF1A	4.16	19.18	High	Medium	
NKF1B	1.9	6.45	Low	Low	
NKF2A	3.84	17.28			
NKF2B	2.59	7.89	Low	Low	
NKF3A	4.39	17.39	Medium	Medium	
NKF3B	2.32	11.9	Low	Low	
NKF4A					
NKF4B	3	9.23	Low	Low	Yellow Ochre
Teleco-Bokazo (TB)					
TB1	4.13	18.91	Low	High	White
TB2	2.26	25	Low	High	White
TB3	3.46	26.24	Low	High	White
TB4	2.51	25.21	Low	High	White
Central Region					
Abonku (AB)					
AB1	6.12	18.11	High	High	Brown
AB2	6.37	18.75	High	High	Light Brown
AB3	4.68	14.28	High	High	Light Brown
Pomase (PM)					
PM1	4.56	20	Low	High	
PM2	3.54	20	High	Low	Silvery Beige
PM3	2.92	8.11	High	Low	Silvery Green
Basofi-Ningo (BN)					
BN1	4.33	13.33	Low	Medium	Light Mangolia
BN2A	2.14	2.4	Low	Medium	Near White
BN2B	4.16	14.62	High	Medium	Greyish White

BN2C	4.36	0	High	Medium	Greyish White
Cape Coast (QP)					
QP	2.18	5.19	Low	Low	Near White
Eastern Region					
Amanfrom (AKA)					
AKA3B		8.4	Low	Low	
Asuboa (AS)					
AS1A		11.8			
AS1B		20	Low	Low	Earthy
AS2A		17.07	Low	Low	Dark Green
AS2B		17			
AS3B		19	Medium	Low	Millitary Green
Akoasi (AK)					
AKA1		21.43	Medium	Low	Light Brown
AKA2		20	Low	Medium	Earthy
AKA3		18.43			
Ahenasi (AB)					
ABA1A					
ABA1B		13.83	Medium	Low	Dark Green
ABA2A		20	Medium	Low	Green
ABA2B		15.81			
ABA3A		18.92			
Apampatia (APP)					
APP1A		24.37	Low	High	Pink